OPTICAL SPECTROSCOPY AND MICROSCOPY OF METALLIC NANOSTRUCTURES

Klas Lindfors

Dissertation for the degree of Doctor of Science in Technology to be presented with due permission of the Faculty of Information and Natural Sciences for public examination and debate in Auditorium AS1 at Helsinki University of Technology (Espoo, Finland) on the 12$^{\text{th}}$ of August, 2009, at 12 noon.

Distribution:
Helsinki University of Technology
Department of Applied Physics
P.O. Box 3500
FI-02015 TKK
Finland
Tel. +358-9-451 3153
Fax. +358-9-451 3155
Available in pdf format at http://lib.hut.fi/Diss

ISBN 978-951-22-9912-6
ISBN 978-951-22-9913-3 (pdf)

Multiprint Oy
Espoo 2009

ABSTRACT OF DOCTORAL DISSERTATION	HELSINKI UNIVERSITY OF TECHNOLOGY P.O. BOX 1000, FI-02015 TKK http://www.tkk.fi

Author Klas Lindfors

Name of the dissertation

Optical spectroscopy and microscopy of metallic nanostructures

Manuscript submitted 12.9.2008	Manuscript revised 10.6.2009
Date of the defence 12.8.2009	
☐ Monograph	☒ Article dissertation (summary + original articles)

Faculty	Faculty of Information and Natural Sciences
Department	Department of Applied Physics
Field of research	Optical Physics
Opponent(s)	Professor Kobus Kuipers
Supervisor	Professor Matti Kaivola
Instructor	Professor Matti Kaivola

Abstract

In this work metallic nanostructures are studied using optical spectroscopy and microscopy. The most striking feature of the optical properties of metallic nanostructures is their capability to support plasmons, coupled oscillations of the conduction electrons and the electromagnetic field. When a plasmon is excited, the optical field can be locally enhanced by orders of magnitude. Also scattering and absorption cross sections increase significantly. These properties open up many interesting applications as well as give information about light-matter interactions on the nanoscale.

Optical microscopy is the natural tool to study the optical properties of nanostructures. The spatial resolution of conventional microscopy is limited to approximately half the wavelength of light. However, by a suitable choice of contrast mechanism, e.g., polarization, wavelength, or degree of polarization, a wealth of information can often be extracted about the nanometer scale details of a structure although they cannot be directly resolved.

In this thesis, optical spectroscopy is combined with microscopy to investigate two types of metallic structures: nanoparticles and slits in metallic thin films. A new method of optical microscopy is developed to make it possible to detect and spectroscopically study individual gold nanoparticles smaller than 10 nm in diameter. The plasmon resonances of such particles are researched using the developed technique. The light transmission properties of narrow slits fabricated in gold thin films are also investigated using methods of optical microscopy. It is shown that the transmission spectrum exhibits resonances whose properties sensitively depend on the dimensions of the structure. Furthermore, the influence of an external disturbance on the transmittance spectrum is studied, an important question for applications in sensing and optical switching. Results of numerical calculations are compared with the experimental data and a good agreement is found.

The central element of any microscopy system is the focusing optic. In this thesis the focusing of partially polarized light is studied theoretically. It is observed that, strikingly, light may become locally fully polarized even when the incident optical field is unpolarized. This counter intuitive effect is confirmed by experiments.

Keywords optical microscopy, optical spectroscopy, plasmon

ISBN (printed)	978-951-22-9912-6	ISSN (printed)	
ISBN (pdf)	978-951-22-9913-3	ISSN (pdf)	
Language	English	Number of pages	67
Publisher	Helsinki University of Technology		

Print distribution

☒ The dissertation can be read at http://lib.tkk.fi/Diss/

VÄITÖSKIRJAN TIIVISTELMÄ	TEKNILLINEN KORKEAKOULU PL 1000, 02015 TKK http://www.tkk.fi

Tekijä Klas Lindfors

Väitöskirjan nimi
Metallisten nanorakenteiden optinen spektroskopia ja mikroskopia

Käsikirjoituksen päivämäärä 12.9.2008	Korjatun käsikirjoituksen päivämäärä 10.6.2009
Väitöstilaisuuden ajankohta 12.8.2009	
☐ Monografia	☒ Yhdistelmäväitöskirja (yhteenveto + erillisartikkelit)

Tiedekunta	Informaatio- ja luonnontieteiden tiedekunta
Laitos	Teknillisen fysiikan laitos
Tutkimusala	Optinen fysiikka
Vastaväittäjä(t)	Professori Kobus Kuipers
Työn valvoja	Professori Matti Kaivola
Työn ohjaaja	Professori Matti Kaivola

Tiivistelmä

Väitöskirjassa tutkitaan metallisia nanorakenteita optisen spektroskopian ja mikroskopian keinoin. Metallien optisista ilmiöistä yksi tärkeimmistä on plasmoniaalto, joka on materiaalin johtavuuselektronien ja sähkömagneettisen kentän kytketty värähtelytila. Valon vuorovaikuttaessa rakenteen kanssa plasmonitaajuudella optinen kenttä voi paikallisesti vahvistua monta kertalukua. Myös valon sironta- ja absorptiovuorovaikutusalat kasvavat merkittävästi. Plasmoneille on suuri määrä mielenkiintoisia sovelluksia, ja ne antavat tietoa valon ja aineen vuorovaikutuksesta nanomittakaavassa.

Optinen mikroskopia on tehokas menetelmä nanorakenteiden optisten ominaisuuksien tutkimiseen. Perinteisen optisen mikroskopian paikkaerotuskyky on rajoittunut noin puoleen valon aallonpituudesta. Tästä huolimatta voidaan sopivaa kontrastimenetelmää hyödyntämällä saada tietoa rakenteen nanometriluokan yksityiskohdista, vaikka niitä ei suoraan pystytäkään erottamaan. Esimerkkejä suureista, joita voidaan hyödyntää, ovat valon polarisaatio, aallonpituus tai polarisaatioaste.

Tässä työssä optisen spektroskopian ja mikroskopian yhdistelmää käytetään kultananohiukkasten ja metalliseen ohutkalvoon valmistettujen nanorakojen tutkimiseen. Työssä kehitetään uudenlainen optisen mikroskopian menetelmä, jolla voidaan havaita yksittäisiä alle 10 nm halkaisijaisia kultananohiukkasia. Menetelmää hyödynnetään väitöskirjassa hiukkasten plasmoniresonanssien tutkimisessa. Toinen tutkimuskohde, jota optisen mikroskopian keinoin työssä tarkastellaan, on kultakalvoon työstetyt muutaman kymmenen nanometrin levyiset raot. Rakojen transmissiospektrissä havaitaan resonansseja, joiden ominaisuudet riippuvat voimakkaasti rakenteen dimensioista. Lisäksi työssä tutkitaan raossa olevan väliaineen taitekertoimen vaikutusta spektriin. Tällä on merkitystä erityisesti anturi- ja kytkinsovelluksissa. Numeerisesti laskettujen transmissiospektrien havaitaan olevan hyvässä sopusoinnussa kokeellisten mittaustulosten kanssa.

Optisessa mikroskopiassa fokusointioptiikka on keskeisessä asemassa. Väitöskirjassa tutkitaan teoreettisesti osittain polaroidun valon fokusointia. Työssä havaitaan, että polaroimaton valo voi johtaa paikallisesti täysin polaroituun valoon linssin polttotasossa. Tämä yllättävä tulos havaitaan työssä myös kokeellisesti.

Asiasanat optinen mikroskopia, optinen spektroskopia, plasmoni

ISBN (painettu)	978-951-22-9912-6	ISSN (painettu)	
ISBN (pdf)	978-951-22-9913-3	ISSN (pdf)	
Kieli	Englanti	Sivumäärä	67
Julkaisija	Teknillinen korkeakoulu		

Painetun väitöskirjan jakelu

☒ Luettavissa verkossa osoitteessa http://lib.tkk.fi/Diss/

To the memory of my mother

Preface

The research summarized in this dissertation has been carried out in the Department of Applied Physics of Helsinki University of Technology (TKK) and the Laboratory of Physical Chemistry of the Swiss Federal Institute of Technology (ETH).

I would like to thank my supervisor and instructor at TKK Prof. Matti Kaivola for his support and patience during the course of this work. I would also like to express my gratitude to Prof. Ari T. Friberg for a very fruitful collaboration. The year 2002 I had the pleasure to work as a visiting researcher in the nano-optics group of Prof. Vahid Sandoghdar at ETH Zürich. During my time in Zürich I learned a great deal about experimental physics and research work in general. I would like to thank Prof. Sandoghdar warmly for giving me this opportunity. During the course of this work I have had the pleasure to collaborate with and to learn from many talented researchers. I would like to thank them for this. I am also grateful to Orvokki Nyberg for taking care of practical matters and the personnel of the workshop of the Department of Applied Physics lead by Seppo Kaivola for helping to realize my ideas.

The research presented in this dissertation has been performed in five different offices and almost as many laboratories. I have thus had the opportunity to interact with a great many people. I would like to thank them for their contribution in both my professional development and for enriching my life outside work too. Both at TKK and in Zürich I have been fortunate to find a group of people interested in physical activities and I would like to thank them for all the hours spent running, skiing or playing different games. In particular Antti H, Timo, Antti J, Alois, and Hannes have contributed greatly in this activity. I would also like to thank my friends for providing a sometimes much needed counterbalance to science.

I wish to thank the Graduate School of Modern Optics and Photonics, TKK, the Academy of Finland, the Jenny and Antti Wihuri Foundation, the Finnish Cultural Foundation, the Vilho, Yrjö and Kalle Väisälä fund, the Ella and Georg Ehrnrooth foundation, and the Finnish Foundation for Technology Promotion for funding my doctoral research.

Throughout my life I have been supported by my family. For this I am deeply grateful to them. Without Ionela this book would never have been

published. I thank her for her love and support during this adventure.

Espoo, June 2009

Klas Lindfors

List of publications

This thesis is a review of the author's work on microscopy and spectroscopy of plasmon resonant nanostructures. It consists of an overview and the following selection of the author's publications in these fields:

I. K. Lindfors, T. Kalkbrenner, P. Stoller, and V. Sandoghdar, "Detection and Spectroscopy of Gold Nanoparticles Using Supercontinuum White Light Confocal Microscopy," *Phys. Rev. Lett.* **93**, 037401 (2004).

II. J. Lindberg, K. Lindfors, T. Setälä, M. Kaivola, and A. T. Friberg, "Spectral analysis of resonant transmission of light through a single sub-wavelength slit," *Opt. Express* **12**, 623–632 (2004).

III. K. Lindfors, L. Lechner, and M. Kaivola, "Dependence of resonant light transmission properties of a subwavelength slit on structural parameters," to appear in *Optics Express* (2009).

IV. K. Lindfors, T. Setälä, M. Kaivola, and A. T. Friberg, "Degree of polarization in tightly focused optical fields," *J. Opt. Soc. Am. A* **22**, 561–568 (2005).

V. K. Lindfors, A. Priimagi, T. Setälä, A. Shevchenko, A. T. Friberg, and M. Kaivola, "Local polarization of tightly focused unpolarized light," *Nature Photonics* **1**, 228–231 (2007).

Throughout the overview, these papers will be referred to by Roman numerals.

Author's contribution

The research presented in this dissertation is the result of work conducted during the years 2001-2008 in the Department of Applied Physics of Helsinki University of Technology (TKK) and the Laboratory of Physical Chemistry of the Swiss Federal Institute of Technology (ETH).

The author has had a key role in all aspects of the research work. He has performed most, and participated in all, of the research in Papers III, IV, and V. The author built the majority of the experimental setup for the study in Paper I and performed the first observations and spectroscopic measurements of nanoparticles down to 10 nm in size. He also played an important role in developing the theoretical model for the interpretation of the results. The study reported in Paper II was designed by the author. He has played a significant role in the interpretation of the results of Papers I, II, IV, and V, and performed all the analysis of the results of Paper III. The author has written Papers III, IV, and V and participated in writing Papers I and II.

Contents

Preface **ix**

List of publications **xi**

Author's contribution **xii**

1 Introduction **1**

2 Theoretical background **5**
2.1 Maxwell's equations 5
2.2 Angular-spectrum representation 6
2.3 Review of basic coherence theory 7
2.4 Transmission of a partially polarized beam through linear, non-image-forming devices 9
2.5 The degree of polarization 10

3 Optical spectroscopy of plasmon resonant nanostructures **13**
3.1 Plasmon resonant nanostructures 13
3.2 Optical properties of metallic nanoparticles 17
3.3 Detection and spectroscopy of single gold nanoparticles with supercontinuum confocal microscopy 23
3.4 Enhanced transmittance of apertures in metal films 29

4 Nano microscopy **37**
4.1 Introduction 37
4.2 Focusing of partially polarized optical fields 39
4.3 Measurement of the local polarization of tightly focused light . 43

5 Summary and conclusions **49**

References **51**

Abstracts of publications I–V **66**

1 Introduction

Nano optics is the field of science that deals with the manipulation and study of optical fields on the nanometer scale as well as with the interaction of light with nanostructures [1–6]. Although it can be justly argued that phenomena classified as nano optical were observed and understood already quite some time ago, the science of nano optics really took off with the development of the near-field optical microscope in 1984 [7,8]. This new tool allowed scientists to perform optical microscopy with a resolution significantly higher than before, opening up a new domain for optical science. This was in itself an important development but more importantly, it has led to a change in our mindset — although the wavelength of visible light is on the order of 500 nm, there is a wealth of optical phenomena occurring at length scales substantially shorter than this.

Among the earliest observations of phenomena firmly belonging to the field of nano optics are the brilliant colours displayed by light scattering from nanometer-sized metal particles as evidenced by the Lycurgus cup from ancient Rome [9]. The scattering is due to the excitation of a resonant oscillation of the conduction electrons of the particles known as a surface plasmon [10]. The study of the optical properties of metallic nanoparticles has drawn considerable interest both theoretically and experimentally. The famous theory of Gustav Mie on light scattering from spherical particles is one of the landmarks of the theoretical work [11]. From an experimental point of view, metallic nanoparticles have attracted much attention both in fundamental studies as well as in applied science [10]. The strong interaction between the electromagnetic field and the particle makes the nanoparticle a convenient system to study light-matter interactions on the nanoscale. At the plasmon resonance, the optical field can be enhanced significantly in the vicinity of the particle. The field enhancement can, e.g., be used to amplify weak processes such as Raman scattering to reach single-molecule sensitivity [12]. The surface plasmon resonance is sensitive to the environment surrounding the particle. This property can be used in sensing applications [13].

In addition to localized plasmons, propagating waves can be excited at metal-dielectric interfaces. Such plasmon polaritons, like their localized counterparts, have attracted great interest over the last decades [14]. The wave propagates along the interface as a combination of charge density oscillation and electromagnetic wave. The plasmon polaritons share many similar properties with localized plasmons. For example, the electromagnetic field is significantly enhanced close to the surface and the resonance is sensitive to changes in the media close to the interface. Furthermore, because the plasmon polariton is localized to the surface but propagates along it, many

additional possibilities for optics using such excitations open up [15–17]. One of the goals of this research has been to develop integrated plasmonic circuits where information is processed by first coupling the input signal to the plasmon polariton, then letting the wave propagate through the device, and finally coupling it out. Basic components such as mirrors and couplers for such devices have already been demonstrated [15–17].

The basic research tool in nano optics is most commonly an optical microscope. The history of microscopy is long and rich and the modern device is not very different from its historical predecessors. It is therefore surprising that optical microscopy has still seen many significant developments in the last decades. The near-field microscope is an important tool in itself but its invention has also spurred the race to develop other novel methods to extend the capability of the optical microscope. Optical microscopy can now, in principle, be performed with arbitrarily good resolution [18]. By combining microscopy with optical spectroscopy, the information obtained is also increased significantly. While a nanostructure might not be directly resolved with a far-field microscope, its spectral response can give important information about the nanometer scale details of the object. Also, the polarization properties are often highly sensitive to the details of the nanostructure.

Most treatments of optical microscopy approximate the electromagnetic field in some way. Commonly, the vectorial nature of light is omitted and the field is taken to be scalar, or, a fully polarized coherent wave is assumed. When these assumptions are abandoned, new interesting phenomena can be expected to be discovered. The field at the focus of a microscope objective displays a complicated three-dimensional (3D) structure where the polarization can change significantly on a scale of tens of nanometers. The coherence and polarization properties of tightly focused light are therefore highly topical questions both for fundamental science as well as for applications. Like the wavelength and polarization, the coherence properties of electromagnetic waves are quantities that characterize optical fields in a fundamental way and can be used to obtain information about the light source or the sample from which the field scatters. Optical coherence is thus a central issue in nano optics.

In this thesis several topics of nano optics are studied. A new method to detect and spectroscopically characterize plasmon resonant metallic nanoparticles is developed. A related nanostructure, a nanoslit in a metal film, is investigated both theoretically and experimentally. Finally, the tight focusing of partially polarized light is treated theoretically as well as experimentally.

The compendium to the thesis is organized as follows: In Sec. 2 some theoretical background to the work is reviewed. The angular spectrum representation of wavefields derived in this section is a powerful tool useful in

treating propagation and focusing of light. Also methods and concepts of second-order electromagnetic coherence theory relevant for this work are reviewed.

Sections 3 and 4 form the core of the work. In Sec. 3 the basic optical properties of metallic nanostructures are briefly discussed. The optics of metallic nanoparticles are then introduced in detail by reviewing the Mie theory. The experimental detection and spectroscopy of gold nanoparticles using supercontinuum light is also presented [Paper I]. The section is concluded by a discussion of the light transmission properties of narrow slits in metal films [Papers II and III].

The focusing of light is the subject of Sec. 4. First the history of microscopy and focusing is briefly reviewed. Then, the theory of focusing partially polarized light is presented in detail [Paper IV]. The focusing of fully polarized waves follows from the general theory as a special case. Finally, a method to study the polarization statistics of optical fields with high spatial resolution is developed and applied to the case of tightly focused light. It is observed that light can become locally polarized in the focal region even when the incident field is unpolarized [Paper V].

2 Theoretical background

The electric current and charge distributions that occur in nature are never fully deterministic but fluctuate randomly to some extent. Furthermore, the electromagnetic fields radiated by these sources can interact with media whose optical properties vary randomly. As a consequence, optical fields also exhibit random fluctuations. In order to analyze the properties of such wave-fields, optical coherence theory is employed. In this section the basic concepts of second-order electromagnetic coherence theory pertaining to partial polarization will be introduced [19–22]. Also basic electromagnetic theory relevant for this work is briefly reviewed [23–25].

2.1 Maxwell's equations

A fluctuating electromagnetic field can be represented by an ensemble of realizations of the field. Throughout the analysis the random quantities are assumed to be stationary with zero mean. When analyzing deterministic fields, each realization can be taken to be the same. A realization of the randomly fluctuating electromagnetic field satisfies the macroscopic Maxwell's equations which in SI units read

$$\nabla \cdot \mathbf{D}(\mathbf{r},t) = \rho(\mathbf{r},t), \tag{1}$$

$$\nabla \cdot \mathbf{B}(\mathbf{r},t) = 0, \tag{2}$$

$$\nabla \times \mathbf{E}(\mathbf{r},t) = -\frac{\partial \mathbf{B}(\mathbf{r},t)}{\partial t}, \tag{3}$$

$$\nabla \times \mathbf{H}(\mathbf{r},t) = \mathbf{j}(\mathbf{r},t) + \frac{\partial \mathbf{D}(\mathbf{r},t)}{\partial t}, \tag{4}$$

where $\mathbf{E}(\mathbf{r},t)$ and $\mathbf{H}(\mathbf{r},t)$ are the electric and magnetic fields, respectively, and $\mathbf{D}(\mathbf{r},t)$ is the electric displacement and $\mathbf{B}(\mathbf{r},t)$ is the magnetic induction. The sources of the electromagnetic field are the free charge density $\rho(\mathbf{r},t)$ and the free current density $\mathbf{j}(\mathbf{r},t)$. These are related by the equation of continuity

$$\frac{\partial \rho(\mathbf{r},t)}{\partial t} + \nabla \cdot \mathbf{j}(\mathbf{r},t) = 0. \tag{5}$$

The response of matter to the electromagnetic field can be described by the electric polarization $\mathbf{P}(\mathbf{r},t)$ and the magnetization $\mathbf{M}(\mathbf{r},t)$. The polarization and magnetization relate the fields to the electric displacement and magnetic induction according to the relations [24]

$$\mathbf{D}(\mathbf{r},t) = \epsilon_0 \mathbf{E}(\mathbf{r},t) + \mathbf{P}(\mathbf{r},t), \tag{6}$$

$$\mathbf{B}(\mathbf{r},t) = \mu_0 \left[\mathbf{H}(\mathbf{r},t) + \mathbf{M}(\mathbf{r},t)\right], \tag{7}$$

where the constants ϵ_0 and μ_0 are the vacuum permittivity and permeability, respectively. In this work we consider the electromagnetic field only in linear, homogeneous, and isotropic media in which case the electric polarization and magnetization are related to the electric and magnetic fields by the following constitutive relations

$$\mathbf{P}(\mathbf{r},t) = \epsilon_0 \int_{-\infty}^{t} \chi(t-t')\mathbf{E}(\mathbf{r},t')\,\mathrm{d}t', \tag{8}$$

$$\mathbf{M}(\mathbf{r},t) = \int_{-\infty}^{t} \eta(t-t')\mathbf{H}(\mathbf{r},t')\,\mathrm{d}t', \tag{9}$$

where $\chi(t)$ and $\eta(t)$ are known as the electric and magnetic susceptibility, respectively. The fact that the polarization and magnetization at time t depend only on the value of the fields at earlier times is simply a statement of causality.

2.2 Angular-spectrum representation

The angular-spectrum representation for the electric field is a useful tool in analyzing wave propagation, scattering, and focusing problems [21, 25]. We consider a monochromatic realization of the electric field oscillating at frequency ω in a source-free region, i.e., $\mathbf{j}(\mathbf{r},t) = \mathbf{0}$ and $\rho(\mathbf{r},t) = 0$. Furthermore, we assume that the response of the material to the electric field can be described by Eq. (8) and that the magnetic susceptibility η is small enough to allow disregarding the magnetization. The latter is usually a good approximation at optical frequencies [24]. With these assumptions we obtain from Maxwell's equations, Eqs. (1)–(4), the Helmholtz equation for the realization of the electric field in frequency space

$$(\nabla^2 + k^2)\mathbf{E}(\mathbf{r},\omega) = \mathbf{0}, \tag{10}$$

where the wave-number of light is defined as $k = n(\omega)\omega/c$, and where $n(\omega)$ is the index of refraction of the medium, and $c = (\epsilon_0\mu_0)^{-1/2}$ is the speed of light in vacuum.

We assume further that the wavefield is propagating into the half-space $z \geq 0$ so that the sources of the field are located in the half-space $z < 0$. We also assume that in any plane $z =$ constant the electromagnetic field can be represented as a Fourier integral, i.e., we write for the electric field

$$\mathbf{E}(\mathbf{r},\omega) = \iint_{-\infty}^{\infty} \hat{\mathbf{E}}(k_x,k_y,z,\omega)\mathrm{e}^{i(k_x x + k_y y)}\,\mathrm{d}k_x\,\mathrm{d}k_y. \tag{11}$$

Inserting this representation into Eq. (10) we obtain a differential equation for $\hat{\mathbf{E}}(k_x, k_y, z, \omega)$ which is readily solved to yield the following representation for $\mathbf{E}(\mathbf{r}, \omega)$,

$$\mathbf{E}(\mathbf{r}, \omega) = \iint_{-\infty}^{\infty} \mathbf{e}(k_x, k_y, \omega) \mathrm{e}^{i(k_x x + k_y y + k_z z)} \, \mathrm{d}k_x \, \mathrm{d}k_y, \tag{12}$$

where

$$k_z = \begin{cases} \sqrt{k^2 - k_x^2 - k_y^2}, & k_x^2 + k_y^2 \leq k^2, \\ i\sqrt{k_x^2 + k_y^2 - k^2}, & k_x^2 + k_y^2 > k^2. \end{cases} \tag{13}$$

Equation (12) is known as the angular spectrum representation of the field and $\mathbf{e}(k_x, k_y, \omega)$ is the angular spectrum in the plane $z = 0$ [21, 25]. Physically, the angular spectrum representation is an expansion of the wavefield in modes. Modes for which k_z is real are simply plane waves traveling in directions specified by the vector $[k_x \; k_y \; k_z]$. The modes for which k_z is imaginary decay exponentially with distance from $z = 0$ and are known as evanescent waves. Here the angular spectrum representation was written for the electric field. The magnetic field can be expressed similarly.

The existence of two types of modes in the angular spectrum representation has physical significance. The propagating plane waves carry the low spatial-frequency information ($k_x^2 + k_y^2 \leq k^2$) whereas the high-frequency information is represented by the evanescent waves. This information is thus lost when the field propagates.

2.3 Review of basic coherence theory

Consider a realization of the fluctuating electromagnetic field $\mathbf{E}(\mathbf{r}, t)$ at point $\mathbf{r}$ and at time t. The polarization properties of the field at a single space-time point are determined by the correlations that exist between the orthogonal field components and are characterized by the equal-time coherence matrix $\mathbf{J}(\mathbf{r})$ whose elements are given by

$$J_{jk}(\mathbf{r}) = \langle E_j^*(\mathbf{r}, t) E_k(\mathbf{r}, t) \rangle, \tag{14}$$

where the angle brackets denote averaging over the ensemble of realizations, the asterisk stands for complex conjugation, and $(j, k) = (x, y, z)$ label the Cartesian components of $\mathbf{E}(\mathbf{r}, t)$ [21]. The coherence matrix does not depend on time t as the fluctuating wavefield was assumed to be stationary. If we furthermore assume that the field is ergodic the ensemble average is equal to the time average [21]. Since fields observed in nature appear to be ergodic,

the polarization properties can experimentally be determined by measuring time averages of the relevant quantities over a long enough period.

The generalization of the equal-time coherence matrix $\mathbf{J}(\mathbf{r})$ is the electric coherence matrix [21] with elements

$$\mathcal{E}_{jk}(\mathbf{r}_1, \mathbf{r}_2, \tau) = \langle E_j^*(\mathbf{r}_1, t) E_k(\mathbf{r}_2, t+\tau) \rangle, \tag{15}$$

which characterizes the correlations that exist between the electric field components at two space-time points $(\mathbf{r}_1, t_1)$ and $(\mathbf{r}_2, t_2)$. Due to stationarity the electric coherence matrix depends on time only through the time difference $\tau = t_2 - t_1$. Similar tensors can be defined to characterize the correlations of the magnetic field components and the correlations between the components of the electric and magnetic fields [21].

It is often more convenient to analyze the electromagnetic field in the space-frequency domain than in the space-time domain. In particular, light-matter interactions are often more simply dealt with in the space-frequency domain as can be seen from the constitutive relations, Eqs. (8)–(9), which are convolutions in the space-time domain. In the space-frequency domain these are multiplications making the analysis simpler. The space-frequency domain analogue to the electric coherence matrix, the cross-spectral density tensor $\mathbf{W}^{(\mathrm{e})}(\mathbf{r}_1, \mathbf{r}_2, \omega)$, is obtained by Fourier transforming Eq. (15) to yield

$$W_{jk}^{(\mathrm{e})}(\mathbf{r}_1, \mathbf{r}_2, \omega) = \frac{1}{2\pi} \int_{-\infty}^{\infty} \mathcal{E}_{jk}(\mathbf{r}_1, \mathbf{r}_2, \tau) \mathrm{e}^{i\omega\tau} \, \mathrm{d}\tau. \tag{16}$$

It can be shown that the cross-spectral density tensor $\mathbf{W}^{(\mathrm{e})}(\mathbf{r}_1, \mathbf{r}_2, \omega)$ can be represented as an average over an ensemble of monochromatic realizations $\{\mathbf{E}(\mathbf{r}, \omega) \exp(-i\omega t)\}$ oscillating at frequency ω [26]. The elements of the cross-spectral density tensor are in this case given by

$$W_{jk}^{(\mathrm{e})}(\mathbf{r}_1, \mathbf{r}_2, \omega) = \langle E_j^*(\mathbf{r}_1, \omega) E_k(\mathbf{r}_2, \omega) \rangle. \tag{17}$$

The polarization properties of the field at a single space-frequency point are determined by the correlations between the field components at that point. By setting $\mathbf{r}_1 = \mathbf{r}_2 = \mathbf{r}$ in Eq. (17) we obtain the spectral coherence matrix $\mathbf{\Phi}(\mathbf{r}, \omega)$ with elements

$$\phi_{jk}(\mathbf{r}, \omega) = W_{jk}^{(\mathrm{e})}(\mathbf{r}, \mathbf{r}, \omega). \tag{18}$$

The spectral coherence matrix is the space-frequency analogue to the equal-time coherence matrix $\mathbf{J}(\mathbf{r})$.

It is to be noted here that so far the electromagnetic field has been assumed to be three-dimensional (3D). In many cases of practical importance the field is beam like so that only two Cartesian vector components are significant. The 2×2 coherence matrix describing the field is in these cases constructed similarly to the full 3×3 coherence matrix from the two non-zero vector components.

2.4 Transmission of a partially polarized beam through linear, non-image-forming devices

The elements of the coherence matrix can for uniformly partially polarized two-dimensional (2D) fields be determined by measuring the intensity of the light after it has been passed through a combination of a retarder and a polarizer oriented in four different orientations [21]. We will now look at how the coherence matrix is transformed when light passes through linear, non-image-forming devices such as a polarizer. It is useful to represent a realization of the fluctuating electric field as a column vector $\mathbf{E}(\omega)$

$$\mathbf{E}(\omega) = \begin{bmatrix} E_x(\omega) \\ E_y(\omega) \end{bmatrix}, \tag{19}$$

where $E_x(\omega)$ and $E_y(\omega)$ are the Cartesian components of the realization. The realization is assumed to be uniform at least over the dimensions of the detector so that no position dependence has been included in Eq. (19). After passing through a linear non-image-forming device the realization is transformed to

$$\mathbf{E}'(\omega) = \mathbf{T}(\omega)\mathbf{E}(\omega), \tag{20}$$

where $\mathbf{T}(\omega)$ is the 2×2 transmission matrix of the device. The coherence matrix of the light transmitted through the device can now be written as

$$\mathbf{\Phi}'(\omega) = \langle \mathbf{E}'^{*}(\omega)\mathbf{E}'^{\mathrm{T}}(\omega) \rangle = \mathbf{T}^{*}(\omega)\mathbf{\Phi}(\omega)\mathbf{T}^{\mathrm{T}}(\omega), \tag{21}$$

where the superscript T denotes the transpose of a matrix and $\mathbf{\Phi}(\omega)$ is the coherence matrix of the light before the device. The transmission matrices for common optical components can readily be written down from the definition of the transmission matrix. For example, a device that has the complex transmission coefficients $t_x(\omega)$ and $t_y(\omega)$ for the x and y components of the field has the transmission matrix

$$\mathbf{T}(\omega) = \begin{bmatrix} t_x(\omega) & 0 \\ 0 & t_y(\omega) \end{bmatrix}. \tag{22}$$

The intensity of the field, or more precisely, the spectral density, is given by the trace of the coherence matrix. From Eq. (21) it is seen that the spectral density $I_{\rm tot}(\omega)$ after the light has been transmitted through a device can be expressed in the form

$$I_{\rm tot}(\omega) = \sum_{ij} R_{ij}(\omega)\phi_{ij}(\omega), \tag{23}$$

where the coefficients $R_{ij}(\omega)$ $(i,j) = (x,y)$ are functions of the elements of the transmission matrix with $R_{xx}(\omega)$ and $R_{yy}(\omega)$ being real valued, and $R_{yx}(\omega) = [R_{xy}(\omega)]^*$. The elements of the coherence matrix can thus be measured by passing the light through suitably chosen optical components and measuring the intensity of the transmitted light to yield four values for $I_{\rm tot}(\omega)$. The elements of the coherence matrix can then be solved for the set of known coefficients $R_{ij}(\omega)$. Most often the intensities of three linearly polarized and one circularly polarized component are measured [21]. The procedure described here is equivalent to measuring the Stokes parameters of the beam.

2.5 The degree of polarization

The degree of polarization is a quantity that reflects the correlations between the electric-field components of the fluctuating electromagnetic wave at a single point. The traditional formulation of this quantity is valid only for beam-like fields, for which the information on the state of partial polarization may be expressed by the 2×2 coherence matrix [21, 22]. Recently, the concept of the degree of polarization was extended to also deal with general 3D electromagnetic wavefields [27] (see also [28]).

The traditional formulation of the degree of polarization is based on uniquely decomposing the 2×2 spectral coherence matrix $\mathbf{\Phi}_2(\mathbf{r},\omega)$ into a sum of two matrices of which one represents unpolarized light and the other one fully polarized light. A natural measure for the degree of polarization is then the ratio of the intensity of the polarized component to the total intensity. The resulting expression for the degree of polarization of a two-dimensional field $P_2(\mathbf{r},\omega)$ is [21, 22]

$$P_2^2(\mathbf{r},\omega) = 1 - \frac{4\det[\mathbf{\Phi}_2(\mathbf{r},\omega)]}{\mathrm{tr}^2[\mathbf{\Phi}_2(\mathbf{r},\omega)]} = 2\left\{\frac{\mathrm{tr}[\mathbf{\Phi}_2^2(\mathbf{r},\omega)]}{\mathrm{tr}^2[\mathbf{\Phi}_2(\mathbf{r},\omega)]} - \frac{1}{2}\right\}, \tag{24}$$

where det and tr denote the determinant and trace of a matrix, respectively. The degree of polarization is bounded between 0 and 1, which correspond to unpolarized and fully polarized fields, respectively. Since the degree of polarization depends only on the trace and determinant of the spectral coherence

matrix, it is invariant under unitary transformations such as rotations of the coordinate system about the beam's propagation direction.

For 3D fields the decomposition of the 3×3 coherence matrix $\mathbf{\Phi}_3(\mathbf{r},\omega)$ into unpolarized and polarized parts is not possible [27]. In this case the concept of the degree of polarization can be formulated in terms of the 3D Stokes parameters [27]. The resulting expression for the 3D degree of polarization, $P_3(\mathbf{r},\omega)$, is

$$P_3^2(\mathbf{r},\omega) = \frac{3}{2}\left\{\frac{\mathrm{tr}[\mathbf{\Phi}_3^2(\mathbf{r},\omega)]}{\mathrm{tr}^2[\mathbf{\Phi}_3(\mathbf{r},\omega)]} - \frac{1}{3}\right\}. \tag{25}$$

The 3D degree of polarization is, as its 2D counterpart, independent of the orientation of the coordinate system and bounded between 0 and 1, which correspond to unpolarized and fully polarized 3D fields, respectively.

The degree of polarization, in both 2D and 3D, is a measure of the average correlation between the field components. This can be seen by expressing it explicitly in terms of the complex correlation coefficients $\mu_{ij}(\mathbf{r},\omega)$ defined as

$$\mu_{ij}(\mathbf{r},\omega) \equiv \frac{\phi_{ij}(\mathbf{r},\omega)}{[\phi_{ii}(\mathbf{r},\omega)\phi_{jj}(\mathbf{r},\omega)]^{1/2}}. \tag{26}$$

The magnitude of the correlation coefficients, i.e., the degree of correlation, is bounded to the interval $0 \leq |\mu_{ij}(\mathbf{r},\omega)| \leq 1$ with the lower limit indicating uncorrelated field components and the upper limit corresponding to complete correlation between the components. Unlike the degree of polarization, the correlation coefficients depend on the orientation of the Cartesian coordinate system. In terms of the degrees of correlation, we can write the 3D degree of polarization as [27]

$$P_3^2(\mathbf{r},\omega) = 1 - \frac{\sum\limits_{ij} 3[1-|\mu_{ij}(\mathbf{r},\omega)|^2]\phi_{ii}(\mathbf{r},\omega)\phi_{jj}(\mathbf{r},\omega)}{[\phi_{xx}(\mathbf{r},\omega)+\phi_{yy}(\mathbf{r},\omega)+\phi_{zz}(\mathbf{r},\omega)]^2}, \tag{27}$$

where the summation is carried out over index pairs $(ij) = (xy, xz, yz)$. A similar expression can also be obtained for $P_2(\mathbf{r},\omega)$. We see from Eq. (27) that if the coordinate system is rotated so that the diagonal elements of the spectral coherence matrix are all equal, which can always be done, the degree of polarization is simply the average of the squared degrees of correlation $|\mu_{ij}(\mathbf{r},\omega)|^2$. A more comprehensive discussion of the 2D and 3D degrees of polarization is given in [27, 28].

3 Optical spectroscopy of plasmon resonant nanostructures

The interest in nanoscience and nanotechnology has fuelled the development of advanced fabrication techniques as well as methods to characterize nanostructures. Optical techniques to observe nanometer sized objects are particularly attractive as the need for sample preparation is often minimal and observations can be made nondestructively. The diffraction limit of optical imaging, however, limits the amount of information that can be obtained by intensity measurements. Near-field techniques such as scanning near-field optical microscopy (SNOM) surpass the resolution limit but are often cumbersome and are restricted to the surface of the sample. Optical spectroscopy, on the other hand, can be used to yield information about subwavelength structures using far-field optics. The spectrum often depends sensitively on the nanometer scale details of the sample. In this chapter we discuss some methods to study two types of nanostructures: gold nanoparticles and nanostructured gold films.

3.1 Plasmon resonant nanostructures

The optical properties of metals are dominantly due to the response of the free conduction electrons to light. The conduction electrons of the metal can be viewed as an electron gas of density n superposed on the positively charged lattice. A simple way to describe the response of the electron gas to an applied electromagnetic field is the Drude model [6]. In the Drude model the electrons are assumed to be displaced from their equilibrium position by $\mathbf{r}$ due to the applied electric field $\mathbf{E}$. The motion of the electrons is also influenced by scattering processes which are described by a damping force written as $-\Gamma m\dot{\mathbf{r}}$, where m is the effective mass of the electron and Γ is the damping constant. The equation of motion for the electrons then becomes

$$m\ddot{\mathbf{r}} = -\Gamma m\dot{\mathbf{r}} + e\mathbf{E}, \tag{28}$$

where e is the electron charge. For a time-harmonic electromagnetic field of angular frequency ω, Eq. (28) can be solved to obtain the following expression for the induced polarization $\mathbf{P}(\omega)$

$$\mathbf{P}(\omega) = -\frac{ne^2/m}{\omega^2 + i\omega\Gamma}\mathbf{E}(\omega). \tag{29}$$

Using Eq. (29) we obtain an expression for the electric susceptibility $\chi(\omega)$ in the frequency domain [see Eq. (8)], so that the relative permittivity $\epsilon(\omega) =$

$1 + \chi(\omega)$ of the electron gas can be written as

$$\epsilon(\omega) = \epsilon'(\omega) + i\epsilon''(\omega) = 1 - \frac{\omega_\mathrm{p}^2}{\omega^2 + \Gamma^2} + i\frac{\omega_\mathrm{p}^2\Gamma}{\omega(\omega^2 + \Gamma^2)}, \tag{30}$$

where the frequency $\omega_\mathrm{p} = \sqrt{ne^2/m\epsilon_0}$ is called the plasma frequency of the metal, and $\epsilon'(\omega)$ and $\epsilon''(\omega)$ are the real and imaginary parts of the permittivity, respectively. From Eq. (30) we see that the real part of the permittivity $\epsilon'(\omega)$ may be negative. For example, for gold $\omega_\mathrm{p} = 13.8 \times 10^{15}$ s^{-1} and $\Gamma = 1.1 \times 10^{14}$ s^{-1} so that $\epsilon'(\omega) < 0$ for visible wavelengths [2]. It is to be noted that the Drude model ignores the influence of the bound electrons which can be signficant. Nevertheless, the model is quite accurate for some metals, particularly in the infrared spectral region, and thus widely used in optics.

From Eq. (30) we observe that for low frequencies the permittivity is dominated by the imaginary part, which is related to dissipation of energy [24], so that light does not penetrate significantly into the medium. For frequencies higher than the plasma frequency $\epsilon'(\omega) > 0$. If the imaginary part of the permittivity is small, the metal is transparent and light can propagate significant distances in it [29]. An incident field oscillating at the plasma frequency, on the other hand, may induce a charge-density oscillation known as a volume plasmon in the medium [29]. Since the volume plasmon is longitudinal it cannot be excited directly with propagating light.

The possibility to excite plasmons is one of the most fascinating features of the optical properties of metals. In addition to the volume plasmons introduced above, plasmons localized in one or more dimensions can also be excited. The condition for this is that the real part of the permittivity is negative and the imaginary part is small [10, 14]. This will be seen explicitly for the case of spherical metal particles in Sec. 3.2. From Eq. (30) we see that in the Drude model the requirement of negative real part of the permittivity is satisfied for frequencies below the plasma frequency. In the visible part of the spectrum silver and gold have both a small imaginary part of the permittivity and a negative real part making them good choices for fabricating structures capable of supporting plasmons. The localized plasmons can be classified into two categories, surface plasmon polaritons (SPPs) which propagate along a metal-dielectric interface and localized surface plasmons (LSPs) confined to nanostructures [6]. Research in the field of optics making use of plasmons has progressed rapidly in recent years and developed into a field of its own known as plasmonics [2, 15–17] in analogue to electronics and photonics.

Plasmons have many attractive properties for both fundamental scientific inquiry as well as for applied research [2, 14–17]. The properties of plasmons,

e.g., the wavelength or propagation length, depend sensitively on the properties of the materials involved. Thus plasmons offer a means to perform materials research. Furthermore, electromagnetic fields can be significantly enhanced close to the metal surface which can be used to amplify weak processes. This has significant implications for both fundamental research and applications. The fact that plasmons can be localized opens the way for many interesting applications. Surface plasmon polaritons are bound to the surface of the metal, a property that has made them an attractive candidate for realizing integrated photonics components. Plasmons excited in metal particles, on the other hand, make the particles appear very bright in scattering experiments which can be utilized in labeling and tracking applications. Finally, the sensitivity of plasmon excitations on the properties of the surrounding media naturally leads to applications in sensing.

One of the challenges in plasmonics research has been to develop methods to optically study isolated metal particles [30]. Achieving this goal is important because it would improve existing or open up new applications as well as making it possible to study fundamental problems such as quantum size effects [10]. Gold nanoparticles can be detected optically either by observing the light scattered by the particle or by detecting light absorption. Recently, also the luminescence from metallic nanoparticles has been observed [31–34]. The detection of the scattered light is hampered by the fact that the Rayleigh scattered light cannot be spectrally separated from the incident field. For gold nanoparticles larger than 40–50 nm in diameter, individual particles can be observed with dark-field or total internal reflection (TIR) microscopy which provides very low background light [35–37]. Also SNOM has been used to detect and study gold nanoparticles. In this case the nanoparticle acts as a scatterer radiating the evanescent light emanating from the SNOM probe tip [38, 39].

As the scattering cross section of a nanoparticle is proportional to the sixth power of the particle radius, the power of the scattered light quickly decreases below the detection limit as the radius is decreased. To increase the amount of scattered light one can make use of very bright light sources such as supercontinuum light generated in a photonic crystal fibre (PCF) [Paper I]. Furthermore, by detecting the scattered light interferometrically the signal is greatly increased [Paper I, 40–44].The strength of the field is proportional to the cube of the diameter of the particle. Interferometric methods can also be used to obtain information about both the real and imaginary parts of the refractive index of the particles [40–43].

In order to reduce the background that hampers the direct detection of the light scattered by a gold nanoparticle, nonlinear techniques can be applied. Both second and third harmonic generation has been observed from

metallic nanoparticles [32, 45, 46]. Second harmonic generation, however, is not possible from spherically symmetric particles which restricts the usability of this method.

The direct observation of absorption of light in metallic nanoparticles is difficult due to the small amount of energy that is absorbed from the illuminating field. On the other hand, absorption dominates scattering for very small particles as the absorption cross section scales as the cube of the radius of the particle. Furthermore, absorbing particles can be distinguished from dielectric scatterers which is particularly important in biological labeling applications. Individual gold and silver nanoparticles have been detected indirectly by a photothermal method in which the thermal lens created by an absorbing particle is observed [47–49]. Recently light absorption in gold nanoparticles has also been observed directly [50].

Smooth and structured metal films have attracted considerable interest in particular for applications in developing integrated devices making use of plasmons [15–17]. Basic components such as switches and reflectors have already been demonstrated [15–17]. One of the most spectacular results of this research is the observation of extraordinary optical transmission (EOT) by Ebbesen *et al.* [51]. In EOT a noble metal film perforated by a periodic array of holes of subwavelength diameter transmits, for certain resonant wavelengths, more light than impinges on the holes.

The extraordinary optical transmission can be understood to be a consequence of light coupling to the plasmon propagating along the patterned incident surface. A similar plasmon can be excited on the other interface. The plasmons are coupled via the holes in the film resulting in the observed enhanced transmission [17]. In addition to increasing the coupling strength between the plasmons propagating on the two interfaces, the periodic pattern of holes provides the necessary momentum to couple the incident propagating light to the plasmon. For smooth surfaces the wavenumber, or momentum, of the plasmon is always greater than that of light and hence propagating electromagnetic fields do not couple to SPPs directly [14].

The basic features of the extraordinary optical transmission effect have after its discovery been intensively researched in the optical and also other wavelength regions both theoretically and experimentally [17, 52–73]. The influence of an array as well as of a single aperture in a metal film on the fluorescence of molecules has been studied [74–77]. By patterning the metal surface around a single aperture it has been shown that the transmission spectrum can be tuned and that the radiation emerging from the aperture can be collimated in the form of a beam [78, 79]. Furthermore, the ability to tune the transmission resonance wavelength has been used to demonstrate switches, including all-optical devices [80–82]. Other applications based on

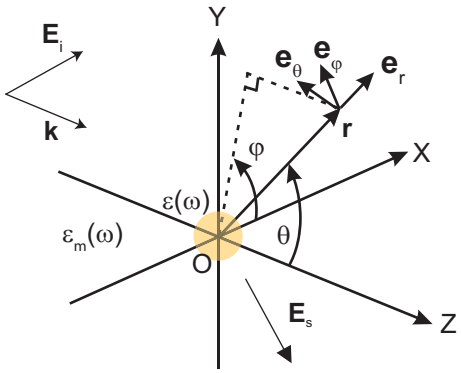

Figure 1: Geometry of scattering of light by a spherical particle. The permittivity of the medium of the particle is $\epsilon(\omega)$ and that of the surrounding region is $\epsilon_{\mathrm{m}}(\omega)$. The polarization of the incident wave $\mathbf{E}_{\mathrm{i}}$ is along the x-axis and the wavevector is along the z-axis. The scattered field is denoted by $\mathbf{E}_{\mathrm{s}}$.

the EOT effect that have been investigated include photodetectors [83, 84], laser [85], wavelength de-multiplexer [86], organic light-emitting diode [87], and sensors [88, 89]. The possibility to use a perforated metal film for imaging and lithography has been studied both experimentally [90] and theoretically [91]. The fact that at the resonance frequency the electromagnetic field can be considerably enhanced in the structure has been applied in non-linear optics [92] as well as in surface enhanced spectroscopy [93, 94].

In the next two sections we discuss the optical properties of metallic nanoparticles and discuss the detection and spectroscopy of gold nanoparticles using supercontinuum confocal microscopy [Paper I]. Spectroscopy of nanostructured gold films is discussed in Sec. 3.4 [Papers II and III].

3.2 Optical properties of metallic nanoparticles

In this section we review the main results from the Mie theory of light scattering from spherical particles [11]. The notation and conventions follow the book of Bohren and Huffman [95]. All the media are assumed to be linear, isotropic and homogenous. We furthermore assume that the magnetic susceptibility of the materials is small enough to be disregarded. The scattering geometry is shown in Fig. 1. A monochromatic electromagnetic plane wave, $\mathbf{E}_{\mathrm{i}}$, oscillating at frequency ω incident along the positive z-axis scatters from a spherical particle of radius a and permittivity $\epsilon(\omega)$. To simplify the notation we only show explicitly the frequency dependency of the material parameters. The coordinate system is defined by the orthogonal axes OX, OY, OZ, and the origin O which is at the center of the particle. Spherical

polar coordinates (r, θ, φ) are introduced with the polar axis along the z-axis and the azimuth φ measured from the OX direction. The basis vectors of the coordinate system are denoted by $\mathbf{e}_{\mathrm{r}}$, $\mathbf{e}_\theta$, and $\mathbf{e}_\varphi$. The permittivity of the medium surrounding the particle is $\epsilon_{\mathrm{m}}(\omega)$ and the scattered field at point $\mathbf{r}$ is denoted by $\mathbf{E}_{\mathrm{s}}(\mathbf{r})$. We furthermore assume that the surrounding medium is nonabsorbing. The polarization of the incident field is taken to be along the x-axis and the amplitude of the field is E_0.

The electromagnetic field must satisfy the Helmholtz equation, Eq. (10), both inside and outside the particle. The field scattered by the spherical particle can be determined by expressing the incident and scattered fields as well as the field inside the particle in terms of a suitable set of basis functions that are solutions to the vector Helmholtz equation. Applying the continuity conditions for the optical field at the surface of the particle yields the expansion coefficients and thus the solution. In the spherical geometry the problem is best solved in terms of vector spherical harmonic functions [95]. The field scattered by the particle can after some algebra be written as

$$\mathbf{E}_{\mathrm{s}}(\mathbf{r}) = \sum_{n=1}^{\infty} E_n[ia_n\mathbf{N}_{\mathrm{e}1n}(\mathbf{r}) - b_n\mathbf{M}_{\mathrm{o}1n}(\mathbf{r})], \tag{31}$$

where $E_n = i^n E_0(2n+1)/n(n+1)$ and the vector spherical harmonics $\mathbf{M}_{\mathrm{o}1n}(\mathbf{r})$ and $\mathbf{N}_{\mathrm{e}1n}(\mathbf{r})$ can be written as

$$\mathbf{M}_{\mathrm{o}1n}(\mathbf{r}) = \cos\varphi\pi_n(\cos\theta)h_n^{(1)}(\rho)\mathbf{e}_\theta - \sin\varphi\tau_n(\cos\theta)h_n^{(1)}(\rho)\mathbf{e}_\varphi, \tag{32}$$

$$\begin{aligned}\mathbf{N}_{\mathrm{e}1n}(\mathbf{r}) = {} & \cos\varphi n(n+1)\sin\theta\pi_n(\cos\theta)\frac{h_n^{(1)}(\rho)}{\rho}\mathbf{e}_{\mathrm{r}} \\ & +[\cos\varphi\tau_n(\cos\theta)\mathbf{e}_\theta - \sin\varphi\pi_n(\cos\theta)\mathbf{e}_\varphi]\frac{[\rho h_n^{(1)}(\rho)]'}{\rho},\end{aligned} \tag{33}$$

where

$$\pi_n(\cos\theta) = \frac{P_n^1(\cos\theta)}{\sin\theta}, \tag{34}$$

$$\tau_n(\cos\theta) = \frac{\mathrm{d}P_n^1(\cos\theta)}{\mathrm{d}\theta}, \tag{35}$$

and $\rho = kr$ with $k = \sqrt{\epsilon_{\mathrm{m}}(\omega)}\omega/c$ being the wavenumber of the light in the medium outside the particle. In Eqs. (32) and (33) $h_n^{(1)}(\rho)$ is the spherical Hankel function of the first kind and order n and the prime denotes differentiation with respect to the argument of the function. In the definition of the functions π_n and τ_n, the function P_n^1 is the associated Legendre function

of the first kind of degree n and order 1 [95]. The expansion coefficients a_n and b_n in the expression of the field, Eq. (31), can be written in terms of Riccati-Bessel functions $\psi_n(x)$ and $\xi_n(x)$ in the form [95]

$$a_n = \frac{m\psi_n(mx)\psi_n'(x) - \psi_n(x)\psi_n'(mx)}{m\psi_n(mx)\xi_n'(x) - \xi_n(x)\psi_n'(mx)}, \tag{36}$$

$$b_n = \frac{\psi_n(mx)\psi_n'(x) - m\psi_n(x)\psi_n'(mx)}{\psi_n(mx)\xi_n'(x) - m\xi_n(x)\psi_n'(mx)}, \tag{37}$$

where

$$\psi_n(y) = yj_n(y), \tag{38}$$

$$\xi_n(y) = yh_n^{(1)}(y), \tag{39}$$

and $j_n(y)$ is the spherical Bessel function of the first kind and order n. In Eqs. (36)–(37) the size parameter x and the relative refractive index m are defined as

$$x = ka, \tag{40}$$

$$m = \frac{n(\omega)}{n_{\rm m}(\omega)}, \tag{41}$$

where $n(\omega) = \sqrt{\epsilon(\omega)}$ and $n_{\rm m}(\omega) = \sqrt{\epsilon_{\rm m}(\omega)}$ are the refractive indices of the particle material and the medium around the particle, respectively.

Using the expression for the scattered field, formulae for the extinction, scattering, and absorption cross sections can be derived. The scattering (absorption) cross section $C_{\rm sca}$ ($C_{\rm abs}$) is defined as the ratio of the scattered (absorbed) power to the intensity of the incident field. The extinction cross section $C_{\rm ext}$ is the sum of the scattering and absorption cross sections and describes the overall disturbance in the incident field caused by the particle. Making use of Eq. (31) the following expressions can be derived for the cross sections [95]

$$C_{\rm sca} = \frac{2\pi}{k^2}\sum_{n=1}^{\infty}(2n+1)(|a_n|^2 + |b_n|^2), \tag{42}$$

$$C_{\rm ext} = \frac{2\pi}{k^2}\sum_{n=1}^{\infty}(2n+1){\rm Re}(a_n + b_n), \tag{43}$$

where Re denotes the real part.

The coefficients a_n and b_n in Eq. (31) correspond to the different modes excited in the particle by the incident wave. For very small particles only the

lowest order dipole mode is significant [95]. By expanding the expressions for the coefficients a_n and b_n in a Maclaurin series, it is found that if $|m|x \ll 1$ the dominant term is a_1 for which we find the formula [95]

$$a_1 = -\frac{i2x^3}{3}\frac{m^2-1}{m^2+2} + O(x^5). \tag{44}$$

Inserting the lowest order term of a_1 into the formula for the scattered field, Eq. (31), and using the asymptotic expression of the Hankel function for large values of the argument, we obtain the following formula for the far-field of the light scattered by a small particle ($x \ll 1$)

$$\mathbf{E}_{\mathrm{s}}(\mathbf{r}) = -E_0 i\frac{e^{ikr}}{kr}\frac{3a_1}{2}\mathbf{e}_{\mathrm{r}} \times \mathbf{e}_{\mathrm{r}} \times \mathbf{e}_{\mathrm{x}}. \tag{45}$$

This is exactly the expression of the far field of a radiating dipole if we identify $\mathbf{p} = \epsilon_{\mathrm{m}}(\omega)\alpha(\omega)E_0\mathbf{e}_{\mathrm{x}}$ as the dipole moment induced by the incident field with $\alpha(\omega)$ denoting the polarizability of the particle

$$\alpha(\omega) = 4\pi a^3\frac{\epsilon(\omega)-\epsilon_{\mathrm{m}}(\omega)}{\epsilon(\omega)+2\epsilon_{\mathrm{m}}(\omega)}. \tag{46}$$

We have here used the exact Mie theory to obtain the dipole approximation for the scattering of light by small particles. The assumptions $|m|x \ll 1$ and $x \ll 1$ physically mean that the electric field is constant over the dimensions of the particle and that any changes in the electric field propagate across the particle in a time much shorter than the oscillation period of the electromagnetic field. The problem can thus be viewed as static and one can obtain the expression for the scattered field using an electrostatic approach [95]. The advantage of the electrostatic approach is that it can be used to calculate the field scattered by non-spherical particles. This will be discussed briefly later on.

From Eq. (46) we clearly see that a resonance (surface plasmon resonance) occurs when $\epsilon(\omega) + 2\epsilon_{\mathrm{m}}(\omega) = 0$. The material of the particle embedded in the non-absorbing host thus has to have a negative permittivity for plasmon oscillation. Since $\epsilon_{\mathrm{m}}(\omega)$ is a real number, the imaginary part of the permittivity of the particle will result in a damped resonance. At the plasmon resonance the polarizability increases and, consequently, the strength of the electric field around the particle can be significantly enhanced from that of the incident field. The scattering cross section of different sized gold particles are shown as a function of wavelength in Fig. 2. The cross sections in Fig. 2 have been calculated with the full Mie theory. For the permittivity of gold we have used the data of Ref. [96]. We can see the plasmon resonance at approximately 550 nm wavelength. As the particle size is increased the plasmon

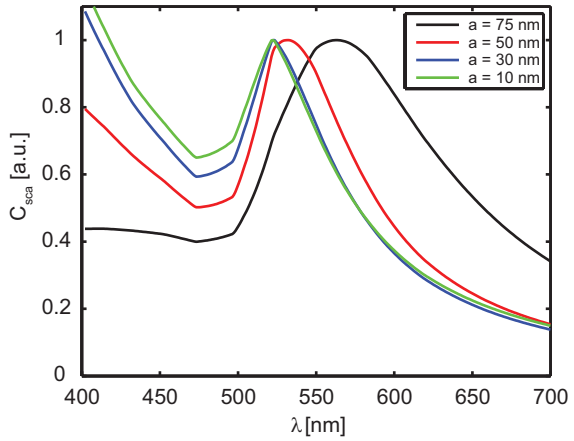

Figure 2: Scattering cross section of a gold nanoparticle as a function of wavelength for four different values of the particle radius a. The external medium is vacuum, $n_{\mathrm{m}} = 1$. The spectra have been normalized by their value at the resonance peak. Ten lowest order modes were included in the calculation.

peak shifts to red as phase-retardation effects become important [10]. There is little difference in the peak position between the 30 nm and 10 nm radius particles. The size of these particles is so small that the interaction between light and the particle can be treated in the electrostatic approximation.

As seen from Eq. (46), a nanoparticle can be used to sense the local refractive index of the material surrounding the particle. Figure 3 shows the scattering spectrum of a 20 nm diameter gold nanoparticle in different dielectric media with constant refractive indices 1, 1.33, and 1.52. As the refractive index of the medium surrounding the particle increases, the plasmon peak shifts to red and also the quality factor of the resonance increases. A layer only a few nanometers thick is enough to produce a significant shift in the resonance wavelength [97]. The shift in the plasmon peak opens up the possibility of constructing microscopic sensors [13, 98, 99]. Biologically interesting molecules have already been detected with such devices [98]. By making use of a single particle, high spatial resolution as well as high sensitivity can be obtained. This approach can also be parallelized with arrays of particles.

The electrostatic approximation can be used to treat also non-spherical particles. One of the simplest non-spherical particles is an ellipsoid. An ellipsoid is also a good model system for more general non-spherical shapes. The electrostatic problem is that of finding the electric field around an ellipsoid with semiaxes a, b, and c placed in a homogeneous static electric field. Similarly to the case of the sphere, we find that in the far zone the particle can be represented as a dipole but now with a diagonal polarizability tensor

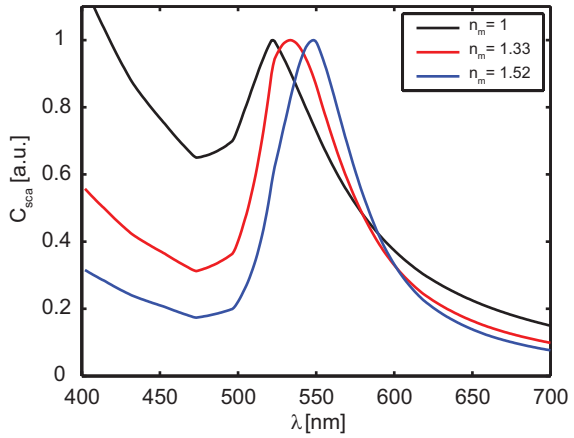

Figure 3: Scattering cross section of a 20 nm diameter gold nanoparticle in different dielectric media with refractive index n_{m}. The spectra have been normalized by their value at the resonance peak. Ten lowest order modes were included in the calculation.

with the diagonal elements [95]

$$\alpha_i = 4\pi abc \frac{\epsilon(\omega) - \epsilon_{\mathrm{m}}(\omega)}{3\epsilon_{\mathrm{m}}(\omega) + 3L_i[\epsilon(\omega) - \epsilon_{\mathrm{m}}(\omega)]}, \quad i = 1, 2, 3. \tag{47}$$

In Eq. (47), the L_i are geometrical factors describing the shape of the particle [95]. The sum of the factors is equal to 1. This model is particularly useful as it can be used to extract information about the shape of individual particles based on measured scattering or absorption data. This was recently experimentally demonstrated in Ref. [100]. From Eq. (47) we also observe that the resonances for different polarizations of the incident field occur at different frequencies. The plasmon resonance for incident light polarized along the short axis of the particle is called transverse plasmon while the plasmon excited when the incident field is polarized along the long axis of the particle is called longitudinal plasmon.

Throughout the previous discussion we have assumed that the incident electromagnetic field is a plane wave. In most applications and in particular in microscopy, however, the optical field is strongly focused. Morita *et al.* studied theoretically the difference between having a plane wave and a focused wave scatter from a particle and concluded that as long as the diameter of the focused spot is larger than 5 times the diameter of the particle the incident field can be taken as a plane wave [101].

3.3 Detection and spectroscopy of single gold nanoparticles with supercontinuum confocal microscopy

In order to avoid ensemble averaging over different sizes and shapes of particles when studying metallic nanoparticles, it is necessary to be able to detect and study individual objects. Furthermore, many applications such as labeling, sensing, or plasmonic devices that make use of the properties of single metal particles benefit from using as small particles as possible. There has thus been a great interest to push the limits of detection toward ever smaller sizes.

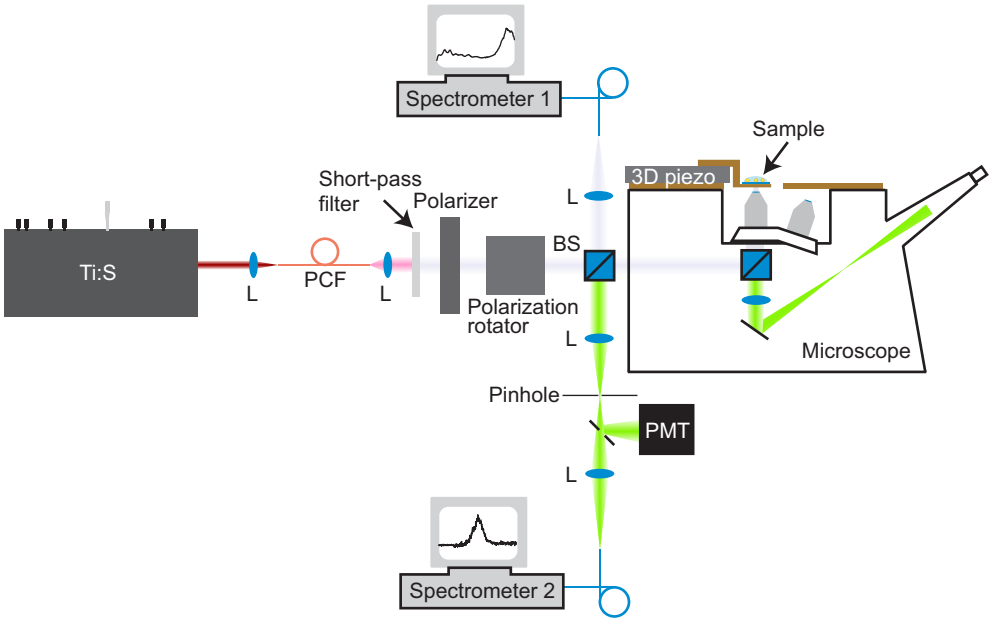

Figure 4: Setup for performing supercontinuum white-light confocal microscopy on gold nanoparticles. Supercontinuum light is generated when an infrared light pulse from a mode-locked titanium:sapphire laser (Ti:S) is passed through a photonic-crystal fibre (PCF). The supercontinuum is collimated using a lens (L), polarized and passed through a polarization rotator and directed into an inverted microscope. Part of the incident light is directed into a spectrometer using a beam splitter (BS). The sample is raster scanned in the microscope using a three-axis piezo-electric positioning system (3D piezo). The backscattered light from the sample is directed from the microscope through a pinhole to either a photomultiplier tube (PMT) or a spectrometer.

Figure 4 shows the confocal microscopy setup used to study light scattering by single gold nanoparticles smaller than 10 nm in diameter [Paper I]. Femtosecond or picosecond near-infrared light pulses from a mode-locked titanium:sapphire laser (Ti:S) are coupled into a single-mode photonic crystal

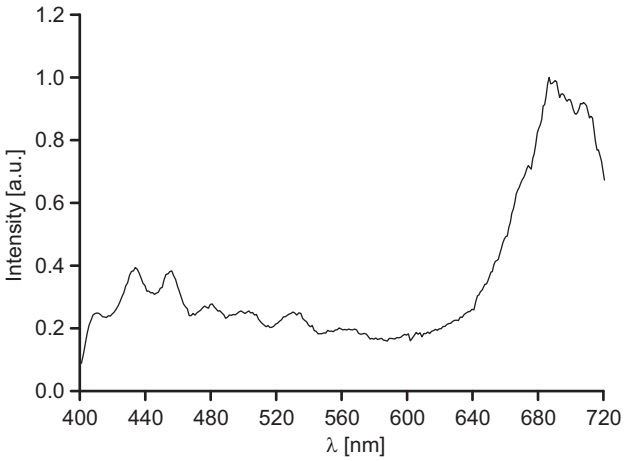

Figure 5: The visible region spectrum of the supercontinuum light when the central wavelength of the incident pulse is 750 nm.

fibre (PCF). The dispersion properties of the fibre have been engineered so that the zero-dispersion wavelength falls within the tuning range of the laser. The low dispersion thus achieved combined with a very small mode volume in the fibre result in strongly nonlinear propagation of the light pulse. As a consequence, the initial narrowband infrared laser pulse is spectrally broadened over the whole visible spectrum and further into the infrared [102]. This supercontinuum light emerging from the fibre is collimated, polarized and directed into an inverted microscope. Part of the incident light is separated and focused into a spectrometer in order to measure the spectrum of the incoming light. This spectrum can be used to normalize the measurements as the supercontinuum light is not spectrally white and also to monitor the performance of the light source. The visible region spectrum of the supercontinuum light is shown in Fig. 5 when the central wavelength of the incident pulse is 750 nm. It is to be noted that the spectrum of the supercontinuum is highly sensitive to the central wavelength of the incident light pulse and to the power coupled into the fibre. In the microscope the light is tightly focused on the sample using a plan apochromatic oil-immersion objective with a numerical aperture of 1.4. The backscattered light is collected and collimated with the same objective and then focused through a pinhole to reduce the background light and directed either onto a photomultiplier tube (PMT) or into a spectrometer equipped with a charge-coupled device (CCD) array.

The samples for the supercontinuum confocal microscopy measurements are made by spin coating a drop of gold nanoparticle solution onto a micro-

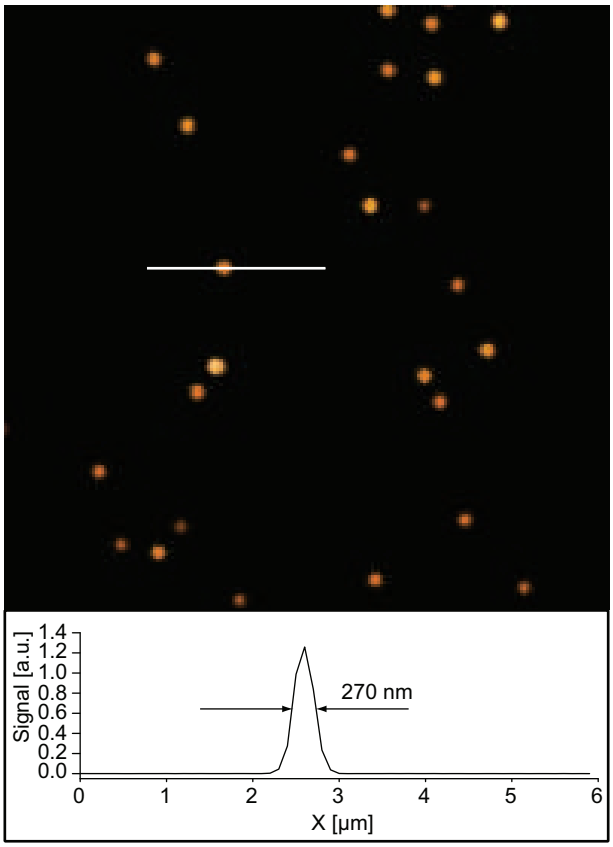

Figure 6: Confocal microscope image of a sample of 60 nm gold nanoparticles. The cross section below the image is along the white line.

scope cover glass. The particles are then covered with immersion oil in order to provide a homogeneous dielectric environment. Figure 6 displays a confocal microscope image of 60 nm gold nanoparticles. A cross section through one of the particles illustrates the excellent focusability of the supercontinuum light. The full-width at half maximum is 270 nm. The particles show similar signal strengths indicating that they are single particles. In addition, scanning electron micrographs of the samples show mainly single particles with only a few aggregates.

To study the spectral properties of the nanoparticles, the scattered light is directed to the spectrometer. Figure 7 shows a typical spectrum obtained for 60 nm gold nanoparticles. The figure displays two spectra corresponding to different particles. The solid line in Fig. 7 corresponds to the Mie spectrum calculated for a spherical gold particle of 60 nm diameter in a medium of refractive index 1.52 using Eq. (42). The theoretically calculated curve was

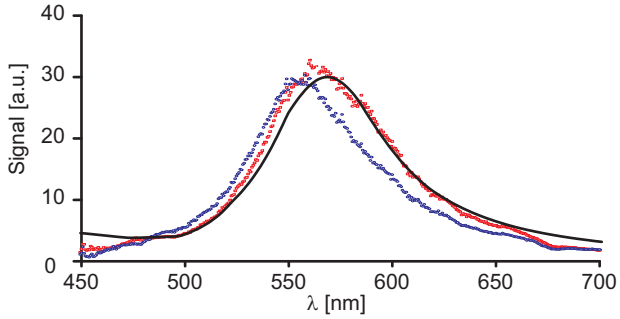

Figure 7: Scattering spectrum of 60 nm gold nanoparticles in immersion oil. The open symbols correspond to two different particles and the solid line is the spectrum calculated with Mie theory using Eq. (42).

scaled to fit the peak height to the measurement data. The agreement between the measured and calculated spectra is quite good. More importantly, the spectra of the two particles are somewhat different. This would not be observable in an ensemble averaged measurement. Small differences in the shape and size of the particles lead to differences in the scattering properties which can be observed in the spectra of individual particles.

As the diameter of the particles decreases, the signal rapidly diminishes. Surprisingly, for small particles the contrast in the confocal images is suddenly reversed as shown in Fig. 8 for 10 nm gold particles. The contrast reversal can be understood with the help of a simple theoretical model [Paper I]. The incident electric field at frequency ω at the focus of the microscope objective is denoted by $\mathbf{E}_{\mathrm{i}}(\omega)$. Part of the incident field is reflected at the glass-oil interface. The reflected light is collimated by the focusing objective and impinges onto the detector. Denoting the reflectivity of the glass-oil interface with r, the amplitude of the reflected field at the detector is $E_{\mathrm{r}}(\omega) = rE_{\mathrm{i}}(\omega)\exp(-i\pi/2)$, where $E_{\mathrm{i}}(\omega)$ is the amplitude of the incident field. The phase shift of $\pi/2$ is the Guoy phase shift accumulated by the beam as it propagates from the focus to the far field [24]. The field scattered by the particle is collimated with the objective and propagates to the detector. We assume that the dipole approximation is valid so that the dipole moment induced by the incident field is $\mathbf{p}(\omega) = [p_x(\omega)\ p_y(\omega)\ p_z(\omega)]^{\mathrm{T}} = \alpha(\omega)\mathbf{E}_{\mathrm{i}}(\omega)$. The geometry is schematically shown in Fig. 9. The far-field radiated by the dipole is given by [see Eq. (45)]

$$\mathbf{E}_{\mathrm{sca}}(\mathbf{r},\omega) = A\frac{e^{ikr}}{kr}\mathbf{e}_{\mathrm{r}} \times \mathbf{e}_{\mathrm{r}} \times \mathbf{p}(\omega), \tag{48}$$

where A is a constant amplitude factor. The objective collimates the scat-

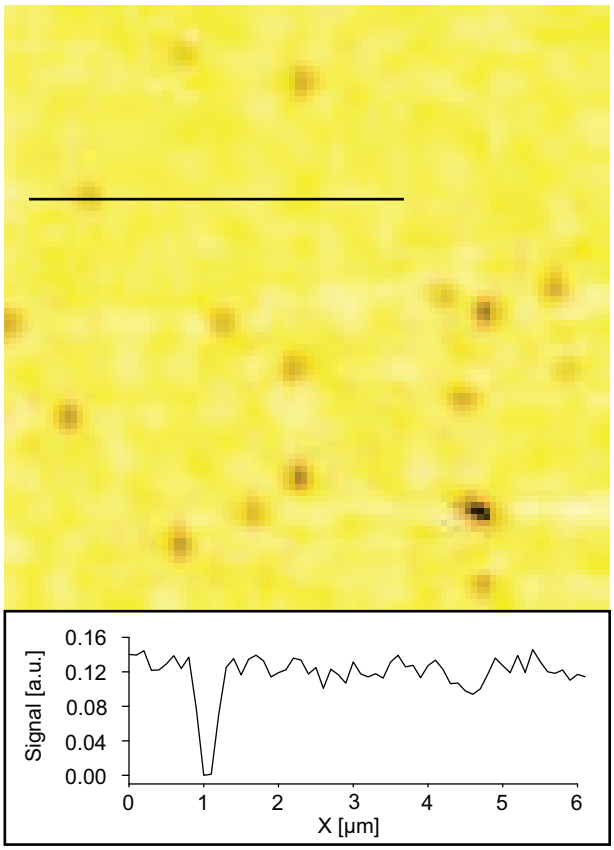

Figure 8: Confocal microscope image of a sample of 10 nm gold nanoparticles. The cross section below the image is along the black line.

tered light into a beam propagating in the direction $\mathbf{k} = \mathbf{e}_z$ along the optical axis. Here $\mathbf{e}_z$ is a unit vector along the positive z-axis. At the objective lens the component of the scattered electric field in the direction of $\mathbf{s}_1 = \mathbf{e}_r \times (\mathbf{e}_r \times \mathbf{k})$ is rotated by refraction to the direction $\mathbf{s}_2 = \mathbf{k} \times (\mathbf{e}_r \times \mathbf{k})$ while the $\mathbf{s}_3 = \mathbf{e}_r \times \mathbf{k}$ component remains unchanged. The collimated field at the lens is thus [103]

$$\mathbf{E}_{\mathrm{coll}}(\mathbf{r},\omega) = [\hat{\mathbf{s}}_1 \cdot \mathbf{E}_{\mathrm{sca}}(\mathbf{r},\omega)]\hat{\mathbf{s}}_2 + [\hat{\mathbf{s}}_3 \cdot \mathbf{E}_{\mathrm{sca}}(\mathbf{r},\omega)]\hat{\mathbf{s}}_3 \tag{49}$$

$$= B\mathbf{A}(\varphi,\theta) \begin{bmatrix} p_x(\omega) \\ p_y(\omega) \\ p_z(\omega) \end{bmatrix}, \tag{50}$$

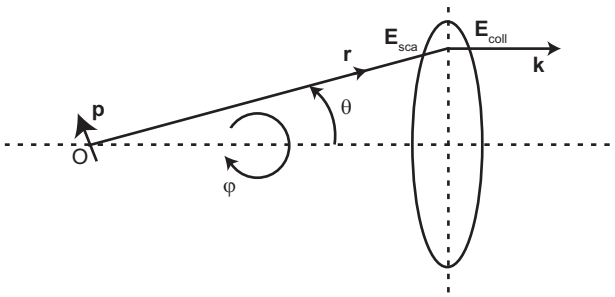

Figure 9: Schematic illustration of the collimation of the light scattered by a dipole $\mathbf{p}$ located at the focus of a microscope objective. The scattered field denoted by $\mathbf{E}_{\mathrm{sca}}$ is collimated with a lens resulting in the field $\mathbf{E}_{\mathrm{coll}}$ with wavevector $\mathbf{k}$ that propagates in the direction of the optical axis.

where the matrix $\mathbf{A}(\varphi, \theta)$ is [103]

$$\mathbf{A}(\varphi,\theta) = \begin{bmatrix} \frac{1}{2}[1+\cos\theta-(1-\cos\theta)\cos 2\varphi] & -\frac{1}{2}(1-\cos\theta)\sin 2\varphi & -\sin\theta\cos\varphi \\ -\frac{1}{2}(1-\cos\theta)\sin 2\varphi & \frac{1}{2}[1+\cos\theta+(1-\cos\theta)\cos 2\varphi] & -\sin\theta\sin\varphi \end{bmatrix}, \tag{51}$$

and B is a constant and the vectors $\hat{\mathbf{s}}_i$ are unit vectors in the directions of $\mathbf{s}_i$ with $i = 1, 2, 3$.

In the experiment, the illumination is linearly polarized so that in the centre of the focal spot the light is linearly polarized in the same direction (see Sec. 4.2). The collimated scattered light is then approximately polarized in the same direction when the particle is in the centre of the focal spot. This can be seen by comparing the total power of the x and y components of the collimated electric field for, e.g., incident light polarized along the x-axis. Even for large numerical apertures the component parallel to the polarization of the incident field dominates. We approximate the collimated scattered field at the detector as a plane-wave with amplitude $E_{\mathrm{coll}}(\omega)$ which is directly proportional to the polarizability of the particle. The amplitude can thus be written as $E_{\mathrm{coll}}(\omega) = \eta\alpha(\omega)E_{\mathrm{i}}(\omega)$ with η being the constant of proportionality. At the detector the scattered and reflected fields interfere and the measured intensity can be written as

$$I_{\mathrm{m}}(\omega) = |E_{\mathrm{coll}}(\omega) + E_{\mathrm{r}}(\omega)|^2 = |E_{\mathrm{i}}(\omega)|^2\{r^2 + |\eta\alpha(\omega)|^2 - 2r\mathrm{Im}[\eta\alpha(\omega)]\}, \tag{52}$$

where Im denotes the imaginary part.

From Eq. (52) we see that the measured signal is composed of three components. The reflected light component, $I_{\mathrm{r}}(\omega) = |rE_{\mathrm{i}}(\omega)|^2$, is present also without a particle and produces a constant background. The light scattered by the particle is represented by the second term, $I_{\mathrm{sca}}(\omega) = |\eta\alpha(\omega)E_{\mathrm{i}}(\omega)|^2$.

This intensity is proportional to $|\alpha(\omega)|^2$ and therefore to a^6. The last term is the interference between the reflected and scattered fields and is proportional to the imaginary part of $\alpha(\omega)$. It therefore scales as a^3. Thus, for large particles the scattering term dominates and the particles are seen as bright. As the diameter of the particle decreases the interference term becomes dominant and the particles appear as dark against the background I_r. The a^3 dependence of the signal in the experiment makes it possible to detect particles smaller than 10 nm in diameter [Paper I]. Furthermore, the spectroscopic data depends on the polarizability, $\alpha(\omega)$, and thus provides information about the shape, size, and material of the particle.

3.4 Enhanced transmittance of apertures in metal films

According to the theory of Bethe on light transmission through a subwavelength hole, the transmittance T of a hole of radius a in a perfectly conducting screen normalized to the aperture area is [104]

$$T = \frac{64}{27\pi^2}(ka)^4. \tag{53}$$

In deriving Eq. (53) the hole radius a is assumed to be much smaller than the wavelength. According to Bethe's theory the transmittance is predicted to be attenuated monotonously as λ^{-4}. The observed enhanced transmittance for perforated noble metal films contradicts this prediction and lead to a flurry of both experimental and theoretical research in the properties of such structures [52–73]. It should, however, be remembered that the original theory of Bethe was derived for applications in the microwave spectral region for which many metals are almost perfect conductors. In the optical domain, however, this assumption is not satisfied [96]. Furthermore, the discovery of EOT was made using periodically patterned surfaces on which propagating light fields can excite SPPs [14]. It is therefore not surprising that the transmittance was observed to be much higher than the value predicted by Eq. (53).

The research into resonant transmission of light through patterned metal films has focused on four different types of structures which are schematically depicted in Fig. 10. For the two-dimensional array of subwavelength apertures, Fig. 10a), the dominant mechanism of light transmission is via excitation of SPPs propagating on the film surface [17, 52, 55, 56, 61, 62, 69]. The experimental research has concentrated on the properties of the structures in the visible and near-infrared spectral regions although the transmission of terahertz waves through hole arrays in doped silicon has also been studied [69]. The importance of SPPs in the transmission process has been demonstrated by measuring the dispersion of the transmission peaks [52] as

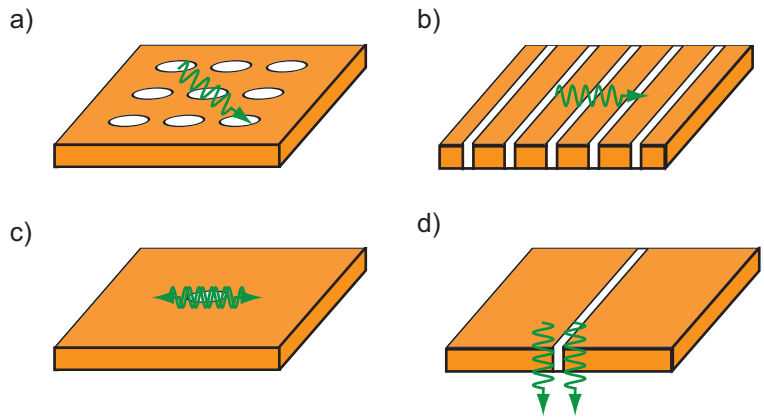

Figure 10: Schematic picture of different types of structures exhibiting resonant optical transmission: a) two-dimensional array of subwavelength apertures, b) grating of narrow slits, c) an isolated subwavelength aperture, and d) an isolated slit.

well as by studying the effect of the properties of the metal surface to the transmittance [55]. Both the dispersion of the transmission peaks and the dependence of the transmittance on the ability to excite a SPP on the surface are in agreement with the model based on the claim that for hole arrays the enhanced transmittance is due to coupling of the two SPP waves on the different sides of the metal film. This view has been confirmed in theoretical studies [61, 62].

The wavelength for which the transmittance is enhanced in a hole array depends on the parameters of the lattice and can thus be tuned [17]. This picture is complicated if the apertures can support propagating modes. This is the case of, e.g., slits or annular apertures [54, 105]. The propagating mode of the structure then provides an additional transmission channel. The grating shown in Fig. 10b) is an example of such a structure where light can excite both SPPs and couple to the mode propagating in the narrow slits. In the microwave region of the electromagnetic spectrum subwavelength gratings can easily be fabricated. In such structures transmittance values of approximately 70 % have been experimentally observed [59]. This experimental observation could be explained by considering just the propagating mode in each slit of the grating. The mode propagates in the slit and is reflected at the film surfaces. This results in Fabry-Pérot type resonances in the transmittance of the structure. The transmission properties of gratings or arrays of structures supporting a propagating mode have in the visible and near-infrared region been intensively investigated theoretically [53, 54, 56–58, 60, 65, 66]. Initially the enhanced transmission was attributed to SPPs being excited on the sur-

face of the grating. Subsequent research identified two mechanisms to be responsible for the light transmission: coupled SPPs on the surfaces of the film and the mode propagating in the slit [54, 56–58, 60]. Later Cao *et al.* have pointed out that for gratings the SPP can actually have a negative impact on the transmittance because the plasmon in effect flies over the slits so that very little light is coupled through the film when a SPP is excited [65].

For individual apertures there is no grating to match the wavevectors of the incident light and the plasmon in order to couple the incident light to SPPs. However, the structure can still support localized plasmons, e.g., a plasmon can be excited at the rim of a cylindrical aperture which can couple to a plasmon on the other side of the film as illustrated in Fig. 10c) [72, 73, 106–108]. The film can also be periodically structured around the aperture so that a SPP can be excited [63]. If the exit surface of the film has such a pattern around the aperture, the light emerging from the aperture can be coupled back to propagating light in the form of a collimated beam [78]. If the isolated aperture supports propagating modes, the incident electromagnetic field may couple to the mode and be transmitted through the film. One of the simplest of such structures is a narrow slit shown in Fig. 10d). For an isolated slit similar Fabry-Pérot type of transmission resonances exist as for gratings [64]. This has been observed first in the microwave region [68] and later in the visible and near-infrared domain [70]. For a slit surrounded by a periodic pattern the transmission is also enhanced when a SPP along the surface is excited on the input side [70].

The measured transmission spectrum of a 26 nm wide and 25 μm long slit in a 193 nm thick gold film is shown in Fig. 11. The slit was fabricated by focused ion beam (FIB) milling of a thermally evaporated gold film. We observe a clear resonance centered at approximately 800 nm wavelength. To make a quantitatively accurate model of the light transmission process, numerical calculations are required [Paper II]. In the particular case of a slit in a metal film, the geometry is invariant in one direction. Maxwell's equations can then be separated into two independent sets of equations [24]. The solutions of these equations are called transverse electric (TE) and transverse magnetic (TM) waves. For TE polarized light the electric field has only one non-zero component whereas for TM waves the same applies for the magnetic field. The general case can be analyzed by decomposing the field into TE and TM polarized waves, significantly reducing the complexity of the problem.

For TE(TM) polarization the complete electromagnetic field is specified by the non-zero electric(magnetic)-field component. The analysis of the light transmission properties of a slit is thus reduced to calculating this scalar field in the structure. A powerful numerical technique to rigorously solve the problem is the boundary-element method (BEM) [109–111]. Starting from

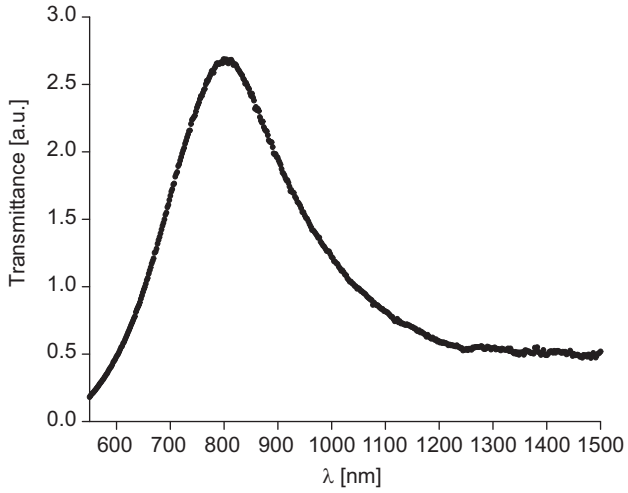

Figure 11: Transmittance of a 26 nm wide and 25 μm long slit milled in a 193 nm thick gold film. The transmittance has not been calibrated absolutely and is thus shown in arbitrary units.

Maxwell's equations an integral equation can be derived for the unknown scalar field. The BEM consists of discretizing the boundaries of regions of homogeneous media in the structure and then solving numerically the scalar field and its derivative normal to the boundary at the discretization points. The homogeneous regions are connected to each other via the boundary conditions of Maxwell's equations. The electromagnetic field in the structure can then be calculated from the boundary values. The BEM leads to a considerable reduction in the resources required for numerical calculations as only the boundaries of the structure need to be discretized. A comprehensive discussion of the boundary integral equation and its numerical implementation is given in Refs. [109–111].

The essential physics involved in light transmission through a subwavelength slit in a metal film can be understood by analyzing the properties of the mode propagating in the slit. For very narrow slits the structure resembles the slab waveguide depicted in Fig. 12. The structure consists of a core of dielectric medium with permittivity $\epsilon_{\mathrm{m}}(\omega)$ surrounded by the metal cladding of permittivity $\epsilon(\omega)$. The coordinate system is shown in Fig. 12. We look for solutions of Maxwell's equations in the form of waves propagating in the direction of the positive z-axis and oscillating at angular frequency ω. The z and time dependence of the field is in this case of the form $\exp[i(k_z z - \omega t)]$ with k_z being the propagation constant of the wave. For TE polarization the non-zero components of the electromagnetic field are E_y, H_x, and H_z. For

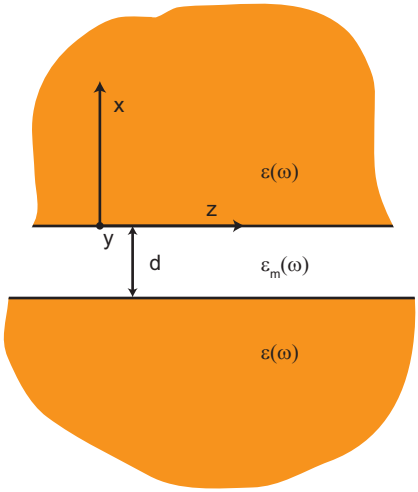

Figure 12: Metal clad waveguide. The thickness of the core with permittivity $\epsilon_{\rm m}(\omega)$ is d. The permittivity of the metal cladding is $\epsilon(\omega)$.

this polarization the waveguide has a cut-off frequency and the imaginary part of k_z grows quickly as the waveguide is made narrower [112]. Consequently, the transmittance of the slit is very low for this polarization [Paper III]. For TM polarization the non-zero field components are H_y, E_x, and E_z. The lowest order TM_0 mode has the special property that it has no cut-off but remains propagating for all values of d. Using Maxwell's equations the following Eigenvalue equation can be derived for $B = (k_z/k)^2$ of the TM_0 mode [112]

$$\frac{2}{\sqrt{\epsilon_{\rm m}(\omega) - B}} \arctan\left[\frac{\epsilon_{\rm m}(\omega)}{\epsilon(\omega)}\sqrt{\frac{B-\epsilon(\omega)}{\epsilon_{\rm m}(\omega)-B}}\right] - kd = 0. \tag{54}$$

Equation (54) can be solved numerically to yield k_z. A physical solution must have both positive real and imaginary part of the propagation constant. The real part of k_z determines the phase change of the mode as it propagates in the waveguide.

The slit structure, Fig. 10d), can be viewed as a section of the slab waveguide where the mode is reflected at the discontinuity at the surfaces of the metal film. The structure then resembles a Fabry-Pérot resonator of length t corresponding to the thickness of the metal film. This model was first analyzed in detail by Takakura [64]. The condition for a resonance can be written as [113]

$$kn_{\rm eff}t + \frac{1}{2}(\phi_1 + \phi_2) = m\pi, \tag{55}$$

where the effective index of the mode is defined as $n_{\text{eff}} = \text{Re}(k_z/k)$, $\phi_{1,2}$ are the phase changes at the reflections from the ends of the waveguide, and m is an integer. The wavelength of the transmission resonance depends on the effective index of the mode as well as on the phase changes $\phi_{1,2}$. Both quantities depend on the width d of the slit [112,113]. The real and imaginary parts of the normalized propagation constant k_z/k are shown in Fig. 13a) as a function of wavelength and the waveguide width for a gold-clad waveguide with core permittivity $\epsilon_{\text{m}}(\omega) = 1$. The imaginary part of the propagation

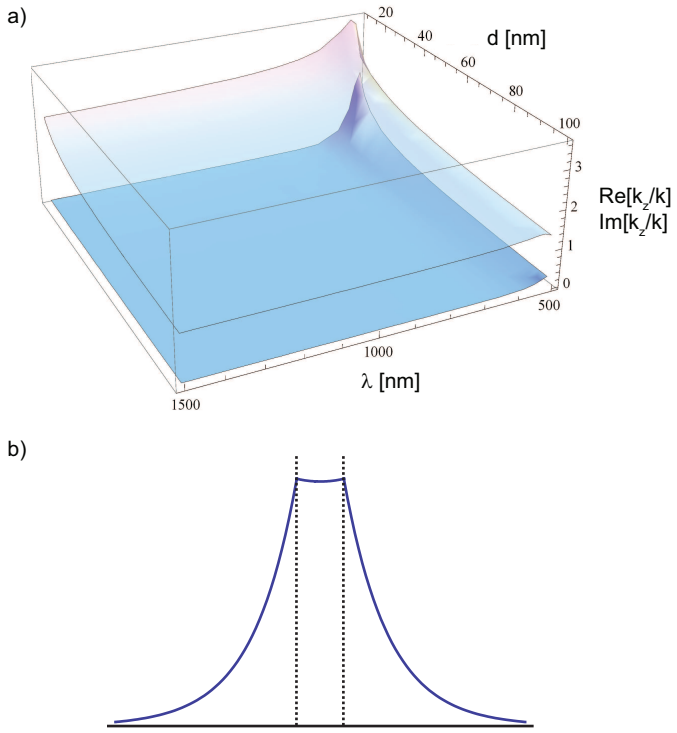

Figure 13: Properties of the TM_0 mode in a gold-clad waveguide: a) the real (upper sheet) and imaginary (lower sheet) part of the normalized propagation constant as a function of wavelength and waveguide width, and b) the real part of the magnetic field in a 26 nm wide waveguide at 800 nm wavelength. In b) the dashed line shows the position of the edges of the core.

constant is seen to be small for near-infrared (NIR) wavelengths and the red part of the visible spectrum, but increasing for shorter wavelengths. This leads to the observed lower transmittance in the visible spectral region than in the NIR [Paper III]. The effective index increases when the waveguide becomes narrower, in particular for visible wavelengths. This results in a

shift of the resonant wavelength [see Eq. (55)]. However, as the phase shift at reflection also depends on the width [113], the evolution of the position of the resonance is not easy to predict quantitatively. A qualitative analysis can be made by using for the phase shifts $\phi_{1,2}$ values calculated using the theory of Ref. [113], and, for the effective index numerically calculated solutions of Eq. (54). For a 193 nm thick gold film the trend for the position of the resonance estimated in this way is to first shift to the blue as the slit becomes narrower. For even narrower slits the resonance then starts to shift toward red. This is in agreement with the experimental data [Paper III]. The higher effective index results in a larger contrast between the waveguide and free space resulting in a higher reflectance for the propagating mode. The Fabry-Pérot resonance should therefore become sharper when d decreases. This has been confirmed by numerical calculations and experiments [Paper II and Paper III].

The real part of the magnetic field of the TM_0 mode of the gold clad waveguide of width 26 nm is shown in Fig. 13b) at the wavelength of 800 nm. The mode is seen to be of surface wave type with field maxima at the interfaces. The mode can be interpreted to be a symmetric superposition of two surface plasmons propagating on the core-cladding interfaces [112]. It is to be noted that the simple waveguide picture for the slit transmittance is only approximative. When the slit becomes wider and the aspect ratio (t/d) lower this model is unlikely to be accurate.

A single slit serves as model system in the analysis of extraordinary optical transmission. By analyzing the dependence of the transmission spectrum as the parameters of the structure are varied, the transmission mechanism can be resolved. Numerically calculated spectra show that the transmittance is similar for different metals indicating that the resonance is a geometrical effect independent of the material parameters [Paper II]. Furthermore, the dependence of the transmission resonance on the dimensions of the structure as well as the input polarization clearly indicate that for individual slits light is transmitted via the propagating mode of the structure [Paper II and Paper III] in agreement with earlier theoretical work [64].

4 Nano microscopy

The word microscopy stems from the Greek words "mikros", meaning "small", and "skopeo" meaning "to view". Microscopy, literally, is the science, and art, of viewing the small. In the previous section spectroscopic methods to gain information about the nanometer scale details of materials and structures were discussed. In this section aspects of optical microscopy pertaining to other properties of light and controlling and studying it on the nanoscale are discussed.

4.1 Introduction

The first usable compound microscopes were probably created by Hans and Zacharias Jansen in Holland around 1590 [114]. The early microscopes were often cumbersome and difficult to use. Anthony Leeuwenhoek was one of the early pioneers who advanced microscopy by making detailed observations of biological samples using his self-made microscopes. Leewenhoek's microscopes were not very different from a powerful magnification glass. The simple early microscopes were improved over the years by advances in optical and mechanical design and fabrication, leading to improved spatial resolution. The next significant development in the history of microscopy was the introduction of achromatic optics to reduce chromatic aberration and the invention of immersion optics by G. B. Amici in 1840 [115].

Until the mid 19th century microscopes were manufactured based on the practical experience of the technicians. The theory of microscope image formation that was developed by Ernst Abbe in 1872 [116, 117] put this activity on an exact mathematical basis and considerably influenced the development of better microscopes. Abbe's theory also showed the limits of resolution in conventional optical microscopy that still remain valid. A similar mathematical theory was developed also by Lord Rayleigh [118]. Later developments in wide-field microscopy have focused on novel contrast mechanisms such as phase contrast [119], dark field [120], differential interference contrast [121], and fluorescence microscopy [122, 123], and, more recently, on novel techniques like photo-activated localization microscopy (PALM) [124], stochastic optical reconstruction microscopy (STORM) [125], and structured illumination microscopy [126], which are all capable of overcoming the diffraction limit.

As shown by Abbe, the resolution of far-field microscopy is limited. The highest spatial frequency components of the scattered or emitted electromagnetic field are evanescent as discussed in Sec. 2.2. As a consequence, in order to surpass the Abbe resolution limit in conventional microscopy it is

necessary to detect also the evanescent waves. The first proposal for such an instrument was made by Synge [127] who suggested to place a local collector in the vicinity of the sample. This idea was first put to practice in the 1970's in the micro-wave region of the spectrum [128]. Soon after the development of the scanning tunneling microscope (STM) [129], a number of other microscopies based on the principle of scanning a local probe over the sample surface emerged [130–135]. Among these were scanning near-field optical microscopy (SNOM) and photon scanning tunneling microscopy (PSTM) which realize the ideas proposed by Synge [7, 8, 136, 137]. In both methods a local probe is raster scanned in the near zone of the sample. The probe provides a means to locally study the electromagnetic field with a resolution that is not limited by diffraction.

Scanning near-field optical microscopy is restricted to studying surfaces and can thus not be used to see into solid samples. Conventional wide-field microscopy, meanwhile, can be used to probe three dimensional (3D) structures but it is not possible to block out-of-focus light which leads to reduced contrast. In effect, light scattered or emitted by all layers of the sample is visible at the same time although only a thin section of the object is in focus. This problem motivated the development of the confocal microscope [138]. In confocal microscopy light from a point source, most often a single transverse-mode laser, is imaged onto the sample in the microscope. The luminescence or scattered light is imaged with the objective and focused onto a photodetector through a pinhole. The pinhole is conjugate to the focal point of the objective lens and efficiently blocks out-of-focus light from reaching the detector. By scanning either the light beam in the microscope or the sample, a three-dimensional image is formed. Confocal microscopy has become a powerful tool in particular in the field of biology due to the 3D imaging capability. Further developments to the basic confocal microscope setup have been made, e.g., by using two-photon excitation [139], parallel imaging [140], and stimulated emission depletion (STED) [18].

In the following section we will study the focusing of light in high numerical aperture (NA) imaging systems such as microscope objectives. In particular, the tight focusing of partially polarized light is considered. A formalism for calculating the coherence matrix in the focal region of a high-NA imaging system is developed. The most important result of this work is the observation that unpolarized light may result in locally fully polarized light in the focal region [Paper IV]. The experimental observation of this is discussed in Sec. 4.3 [Paper V].

4.2 Focusing of partially polarized optical fields

The distribution of light intensity and polarization at the focus of a microscope objective has been studied extensively. Most of the treatments on the focusing of electromagnetic fields have been restricted to deterministic illumination. Some of the earliest theoretical works on the subject were performed by Ignatowsky [141] and Hopkins [142]. Later Richards calculated the intensity distribution along the optical axis for linearly polarized illumination [143]. This work was subsequently expanded by Richards and Wolf to a study on both the intensity and polarization distribution for focused, linearly polarized light. They illustrated the differences between the scalar and electromagnetic approaches [144]. It was found that the rotational symmetry of the intensity distribution is broken in the focal region which has recently also been experimentally observed [145]. This asymmetry of the intensity distribution was also noted by Hopkins [142, 146]. The possibility to realize complicated intensity and polarization patterns at the focus of a high NA objective using suitably polarized illumination has prompted a number of experimental and theoretical studies on the focusing of non-uniformly polarized optical beams [147–157]. To experimentally image the intensity distribution and to study the polarization properties of such field distributions, single molecule imaging [158, 159] and scanning near-field optical microscopy have been used [160, 161]. In applications, the influence of aberrations on the focal region light distribution is particularly important. In microscopy in particular, the refractive index mismatch between the microscope cover glass and the sample results in increased spherical aberration and decreased resolution. This problem as well as focusing into crystalline media has been the topic of a number of studies [162–167].

The focusing of randomly fluctuating electromagnetic waves has attracted less attention than that of deterministic fields. However, in many applications the illumination is not fully deterministic. For example, in microscopy, the illumination is often unpolarized. Most studies on focusing of fluctuating optical fields have been performed within the framework of scalar theory thus omitting the polarization of light [168–170]. As discussed above, many features observed in tightly focused light are related to the vectorial nature of light. The focusing of fluctuating electromagnetic fields is thus a highly topical question.

To study the 3D degree of polarization in the image space of a rotationally symmetric aplanatic optical system, we can extend the Richards-Wolf theory for the focusing of collimated linearly polarized beams [144, 171] to deal with partially polarized incident light [Paper IV]. By calculating separately the electric field in the focal region for both x and y polarized illumination and

by combining the results, we obtain an expression for the coherence matrix of the focal field.

To calculate the field in the focal region of an imaging system we make use of the angular spectrum representation, Eq. (12), for a single monochromatic realization of the field. By Fourier inversion we have from Eq. (12)

$$\mathbf{e}^{\mathrm{inc}}(k_x, k_y, \omega) = \frac{1}{(2\pi)^2} \mathrm{e}^{-ik_z z_0} \iint_{\mathcal{A}} \mathbf{E}^{\mathrm{inc}}(x, y, z_0, \omega) \mathrm{e}^{-i(k_x x + k_y y)} \, \mathrm{d}x\mathrm{d}y, \qquad (56)$$

where $z = z_0$ is a plane where the field is assumed to be known and the superscript inc refers to incident wave. We furthermore have assumed that the field is non-zero only within the aperture $\mathcal{A}$ of the focusing system. In focusing problems the incident field most often corresponds to a converging wave

$$\mathbf{E}^{\mathrm{inc}}(x, y, z_0, \omega) = \frac{\mathbf{E}_0(x, y, z_0, \omega)}{R_1} \mathrm{e}^{-ikR_1}, \qquad (57)$$

where $R_1 = [(x-x_1)^2 + (y-y_1)^2 + (z_0-z_1)^2]^{1/2}$ and the point $\mathbf{r}_1 = (x_1, y_1, z_1)$ is the geometrical focus. Here $\mathbf{E}_0(x, y, z_0, \omega)$ is an amplitude factor. Since the focus is for realistic imaging systems far away from the aperture compared to the wavelength, i.e., $k|z_0 - z_1| \gg 1$, we can evaluate the integral in Eq. (56) asymptotically using the method of stationary phase. If we furthermore make the Debye approximation and only retain the contributions to the integral from the interior stationary points and neglect contributions from the edges of the aperture we obtain [171]

$$\mathbf{e}^{\mathrm{inc}}(k_x, k_y, \omega) = -\frac{i}{2\pi k_z} \mathbf{a}(k_x, k_y, \omega) \mathrm{e}^{-i\mathbf{k}\cdot\mathbf{r}_1}, \qquad (58)$$

where

$$\mathbf{a}(k_x, k_y, \omega) = \mathbf{E}_0[x_1 - (z_1 - z_0)k_x/k_z, y_1 - (z_1 - z_0)k_y/k_z, z_0, \omega], \qquad (59)$$

and $\mathbf{k} = [k_x \ k_y \ k_z]$. Physically the Debye approximation means that only plane wave components within the solid angle Ω subtended by the focusing system aperture contribute to the focal field. The contribution of light diffracted from the edge of the aperture to the angular spectrum is neglected in the Debye approximation. Using the expression of Eq. (58) for the angular spectrum of the converging wave, we can write the field in the focal region as

$$\mathbf{E}(\mathbf{r}, \omega) = -\frac{i}{2\pi} \iint_{\Omega} \frac{\mathbf{a}(k_x, k_y, \omega)}{k_z} \mathrm{e}^{i\mathbf{k}\cdot(\mathbf{r}-\mathbf{r}_1)} \, \mathrm{d}k_x \mathrm{d}k_y. \qquad (60)$$

The form for the focused field that we have obtained in Eq. (60) expresses the field as a superposition of plane waves that converge to the focus.

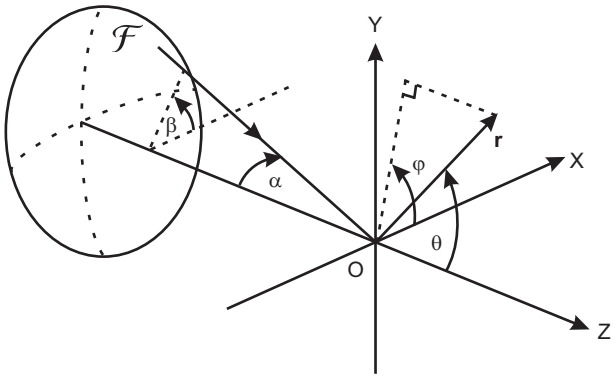

Figure 14: Illustration of the geometry and notations used in the analysis of tightly focused electromagnetic fields.

The amplitude and polarization of each plane wave component is given by $\mathbf{a}(k_x, k_y, \omega)$. In order to calculate the electric field distribution in the focal region, the task is thus simplified to finding these vector amplitudes. We will next use the integral representation of Eq. (60) to calculate the electric field distribution in the focal region for a cylindrically symmetric high-NA imaging system.

To generalize the focusing theory of Richards and Wolf [144] to apply also to fluctuating electromagnetic fields, we consider a planar optical field incident on a cylindrically symmetric aplanatic imaging system along the z-axis, as illustrated in Fig. 14. The origin of the Cartesian coordinate system O is chosen to coincide with the focus and we introduce spherical polar coordinates (r, θ, φ) with the polar axis along the axis of revolution of the system and the azimuth φ measured from the OX direction. The electric field components of the 2D incident field $\mathbf{E}^{\text{inc}}$ are written as

$$\mathbf{E}_i^{\text{inc}}(\mathbf{r}, \omega) = E_i^{\text{inc}}(\omega) A^{\text{inc}}(x, y, \omega) \mathrm{e}^{ikz} \mathbf{e}_i, \quad i = (x, y). \tag{61}$$

In Eq. (61) $A^{\text{inc}}(x, y, \omega)$ is the transverse profile of the wave and assumed to be cylindrically symmetric. The fluctuating nature of the field is incorporated in the amplitude $E_i^{\text{inc}}(\omega)$ which is a random variable. The unit vectors along the Cartesian coordinate axes are denoted by $\mathbf{e}_i$, with $i = (x, y)$.

We first look at the case when the incident field is polarized along the x-axis. Using similar arguments as in Sec. 3.3 when discussing how light is collimated by a lens we find that the polarization vector of the plane wave component with azimuth β and polar angle α (see Fig. 14) is (see also

Ref. [171])

$$\begin{aligned}\mathbf{s}(\alpha,\beta) &= [\cos\alpha+\sin^2\beta(1-\cos\alpha)]\mathbf{e}_{\mathrm{x}}-(1-\cos\alpha)\sin\beta\cos\beta\mathbf{e}_{\mathrm{y}}\\ &\quad+\sin\alpha\cos\beta\mathbf{e}_{\mathrm{z}}.\end{aligned}\tag{62}$$

Due to the cylindrical symmetry of the optical system and the incident field, the amplitudes of the plane wave components converging to the focus depend only on the polar angle α and we can write $\mathbf{a}(\alpha,\beta,\omega)=A(\alpha,\omega)\mathbf{s}(\alpha,\beta)$. Inserting this into Eq. (60) and performing the integration with respect to β we obtain the following expression for the x, y and z components of the focal field produced by the x polarized illumination

$$E_x(\mathbf{r},\omega) = -E_x^{\mathrm{inc}}(\omega)\frac{ik}{2}\left[I_0(\mathbf{r},\omega)+I_2(\mathbf{r},\omega)\cos 2\varphi\right],\tag{63}$$

$$E_y(\mathbf{r},\omega) = -E_x^{\mathrm{inc}}(\omega)\frac{ik}{2}I_2(\mathbf{r},\omega)\sin 2\varphi,\tag{64}$$

$$E_z(\mathbf{r},\omega) = -E_x^{\mathrm{inc}}(\omega)kI_1(\mathbf{r},\omega)\cos\varphi.\tag{65}$$

Here φ is the azimuth at the position $\mathbf{r}$ and

$$I_0(\mathbf{r},\omega) = \int_0^{\alpha_0}A(\alpha,\omega)\sin\alpha(1+\cos\alpha)J_0\left(v\frac{\sin\alpha}{\sin\alpha_0}\right)\mathrm{e}^{iu\frac{\cos\alpha}{\sin^2\alpha_0}}\,\mathrm{d}\alpha,\tag{66}$$

$$I_1(\mathbf{r},\omega) = \int_0^{\alpha_0}A(\alpha,\omega)\sin^2\alpha J_1\left(v\frac{\sin\alpha}{\sin\alpha_0}\right)\mathrm{e}^{iu\frac{\cos\alpha}{\sin^2\alpha_0}}\,\mathrm{d}\alpha,\tag{67}$$

$$I_2(\mathbf{r},\omega) = \int_0^{\alpha_0}A(\alpha,\omega)\sin\alpha(1-\cos\alpha)J_2\left(v\frac{\sin\alpha}{\sin\alpha_0}\right)\mathrm{e}^{iu\frac{\cos\alpha}{\sin^2\alpha_0}}\,\mathrm{d}\alpha,\tag{68}$$

where J_0, J_1, and J_2 are Bessel functions of the first kind, and we have introduced the optical coordinates u and v via the definitions

$$u = \frac{2\pi}{n\lambda_0}z\mathrm{NA}^2,\tag{69}$$

$$v = \frac{2\pi}{\lambda_0}\rho\mathrm{NA},\tag{70}$$

where $\rho=(x^2+y^2)^{1/2}$. The parameters $\mathrm{NA}=n\sin\alpha_0$ and α_0 are the numerical aperture and angular semiaperture of the optical system, respectively, and n is the refractive index of the focal region medium. The explicit form of the function $A(\alpha,\omega)$ in Eqs. (66)–(68) depends on the optical system and the

transverse profile, $A^{\mathrm{inc}}(x, y, \omega) = A^{\mathrm{inc}}(\rho, \omega)$, of the incident electromagnetic field. The assumption of aplanatism means that the imaging system fulfills the sine condition and in this case the expression for $A(\alpha, \omega)$ is [171]

$$A(\alpha, \omega) = A^{\mathrm{inc}}(f \sin\alpha, \omega) \cos^{1/2}\alpha, \tag{71}$$

where f is the focal length of the focusing system.

By repeating the previous analysis for an incident electric field polarized in the y direction, we can express the electric field of the focal region in the form $\mathbf{E}(\mathbf{r}, \omega) = \mathbf{M}(\mathbf{r}, \omega)[E_x^{\mathrm{inc}}(\omega)\ E_y^{\mathrm{inc}}(\omega)]^{\mathrm{T}}$, where the matrix $\mathbf{M}(\mathbf{r}, \omega)$ is

$$\mathbf{M}(\mathbf{r}, \omega) = -\frac{ik}{2} \begin{bmatrix} I_0(\mathbf{r}, \omega) + I_2(\mathbf{r}, \omega)\cos 2\varphi & I_2(\mathbf{r}, \omega)\sin 2\varphi \\ I_2(\mathbf{r}, \omega)\sin 2\varphi & I_0(\mathbf{r}, \omega) - I_2(\mathbf{r}, \omega)\cos 2\varphi \\ -2iI_1(\mathbf{r}, \omega)\cos\varphi & -2iI_1(\mathbf{r}, \omega)\sin\varphi \end{bmatrix}. \tag{72}$$

To obtain the coherence matrix of the light in the focal region we now take the ensemble average to yield the following expression for the coherence matrix in the focal region $\mathbf{\Phi}_3(\mathbf{r}, \omega)$ in terms of the 2×2 coherence matrix $\mathbf{\Phi}^{\mathrm{inc}}(\omega)$ of the incident paraxial field

$$\mathbf{\Phi}_3(\mathbf{r}, \omega) = \mathbf{M}^*(\mathbf{r}, \omega)\mathbf{\Phi}^{\mathrm{inc}}(\omega)\mathbf{M}^{\mathrm{T}}(\mathbf{r}, \omega). \tag{73}$$

Equations (72) and (73) can be used to study the properties of the electromagnetic field in the focal region for arbitrary homogeneous polarization of the incident beam. Figure 15 shows the distribution of the degree of polarization in the focal plane of an imaging system with an NA of 0.9 for unpolarized incident light. We observe that the focus is surrounded by rings on which the field is fully polarized. This surprising phenomenon is a geometric effect. In the focal region the components of the electromagnetic field are linear combinations of the two components of the incident field. On the rings of full polarization the two components contribute in equal proportion to the three components of the focal field. Thus, the x, y, and z components of the focal field are fully correlated and consequently the field is fully polarized [see Eq. (27)].

4.3 Measurement of the local polarization of tightly focused light

To observe unpolarized incident light become polarized in the focal plane of the focusing optic, a technique to probe the polarization statistics with high resolution is required. In optical microscopy the complementary task of determining and controlling the orientation of nanoscopic and microscopic objects by using focused polarized light has already been accomplished by

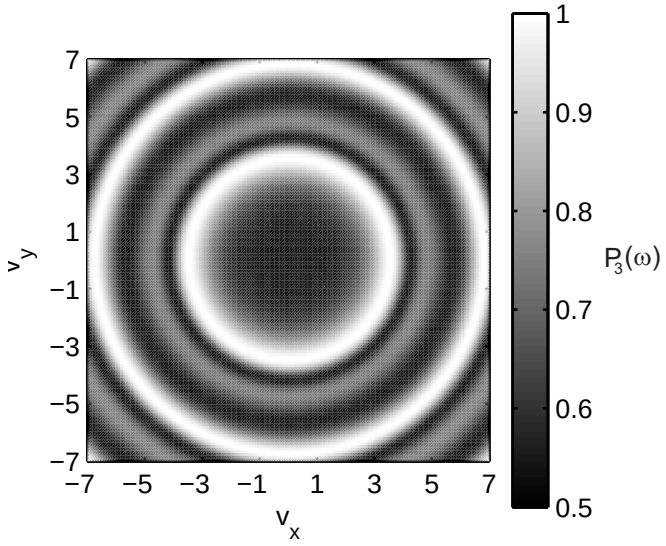

Figure 15: Degree of polarization in the focal plane of an imaging system with an NA of 0.9. The incident light is an unpolarized plane wave and the refractive index of the focal region medium is 1. The axes are defined as $v_\mathrm{x} = v\cos\varphi$ and $v_\mathrm{y} = v\sin\varphi$.

using probes whose response is polarization sensitive [158, 159, 172, 173]. To experimentally determine the polarization statistics with high spatial resolution, a nanoscopic scatterer whose response is polarization insensitive should be used. Spherical gold nanoparticles fulfil these requirements and are thus a good choice to probe the local polarization statistics of optical fields.

Gold nanoparticles have previously been demonstrated as probes in near-field microscopy to map intensity distributions [174]. A spherical nanoparticle with radius much smaller than the wavelength of light can be considered as an electric dipole as discussed in Sec. 3.2. By analyzing the polarization properties of the far-field scattered by the particle, information about the polarization statistics of the field at the position of the particle are obtained. Experimentally, the scattered light is collected and collimated by a lens so that a planar wave field $\mathbf{E}'$ results. The relation between the local field at the position $\mathbf{r}$ of the particle and the collimated field at position $\mathbf{r}'$ is described as in Sec. 3.3 by the matrix $\mathbf{A}(\mathbf{r}')$ of Eq. (51) [103]. The coherence matrix of the collimated field as a function of the coherence matrix of the field at the position of the particle, $\mathbf{\Phi}_3$, can then be expressed as $\mathbf{\Phi}_2(\mathbf{r}', \mathbf{r}, \omega) = |C|^2\mathbf{A}(\mathbf{r}')\mathbf{\Phi}_3(\mathbf{r}, \omega)\mathbf{A}^\mathrm{T}(\mathbf{r}')$. The constant $|C|^2$ can be omitted when analyzing normalized quantities such as the correlations between the field components or the degree of polarization. The scattering process described here is illustrated in Fig. 16.

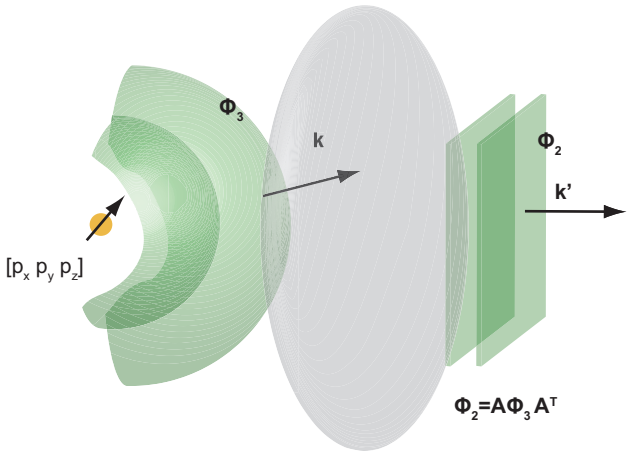

Figure 16: Schematic of the probing of the local polarization properties of a light field with a gold nanoparticle. The incident field induces a dipole moment $\mathbf{p} = [\mathrm{p}_x\ \mathrm{p}_y\ \mathrm{p}_z]$ to the particle. The coherence matrix of the field at the position of the particle is denoted by $\mathbf{\Phi}_3$. The scattered field (wavevector $\mathbf{k}$) is collected with a lens to propagate in a collimated beam of light with wavevector $\mathbf{k}'$ and characterized by the coherence matrix $\mathbf{\Phi}_2$. The scattered light thus carries information about the polarization properties at the position of the particle.

To experimentally observe the effect of light becoming locally polarized when focused [Paper V], a collimated beam of light is produced by splitting a laser beam ($\lambda = 532$ nm) into two orthogonally linearly polarized components and recombining them after one of the beams has been delayed with respect to the other by a distance longer than the coherence length of the light. The laser used in the experiments has a linewidth of 30 GHz corresponding to a coherence length of approximately 10 mm. The recombined beams are then passed through a single-mode optical fiber to make them fully co-propagating. The degree of polarization of the light emerging from the fiber can be controlled by varying the ratio of the intensities of the two incident beams. A tightly focused optical field is produced by directing the light from the fibre to an inverted optical microscope where it is focused with a microscope objective of NA = 1.3. The degree of polarization in the focal region is probed with a single gold nanoparticle as illustrated in Fig. 17.

Samples of nanoparticles are prepared as described in Sec. 3.3. To map the polarization statistics of the focal field, the sample is raster scanned in the focal plane of the focusing objective using a piezo-electric positioning system. A single nanoparticle is positioned close to the focus and the light backscattered from it is collected by the objective, collimated, and directed through an aperture to a polarization analyzer. The aperture is used to

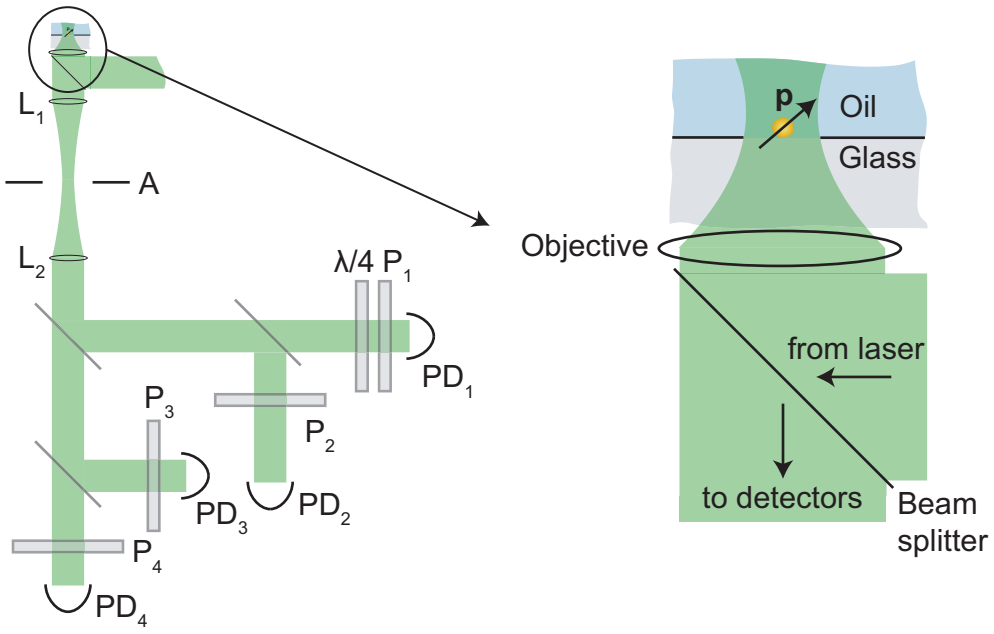

Figure 17: Schematic of the experimental setup. The light backscattered by a single nanoparticle as it is scanned through the focus is collected by the focusing objective, collimated, and directed to a polarization analyzer. In the analyzer the degree of polarization of the scattered light is determined by performing four intensity measurements to obtain the elements of the 2×2 coherence matrix. The analyzer consists of four polarizers P_i, a quarter-wave plate $\lambda/4$, and four identical photodetectors PD_i. The scattered light is passed through an aperture A using two lenses $\mathrm{L}_{1,2}$ to limit the amount of background light reaching the detectors. A drop of immersion oil is applied to the sample to provide a homogeneous environment and to suppress the reflection from the glass surface.

limit the amount of background light reaching the large-area detectors in the polarization analyzer. The aperture is much larger in diameter (200 μm–400 μm) than the image of the particle (≈ 50 μm) so that its influence is just to reduce the background light. The elements of the coherence matrix of the scattered light are determined by performing four intensity measurements as discussed in Sec. 2. The unavoidable slight polarization dependencies of the optical elements in the setup are thoroughly taken into account in the measurements by first calibrating the analyzer using light of known polarization state. This was done by passing to the analyzer linearly polarized light through a quarter-wave plate that was rotated a full circle and fitting a model of the type of Eq. (23) to the response of the detectors with the coefficients R_{ij} as well as the power of the incident light as free parameters. The calibration procedure was confirmed by measuring the polarization state of a number of selected known polarization states of the input light. The con-

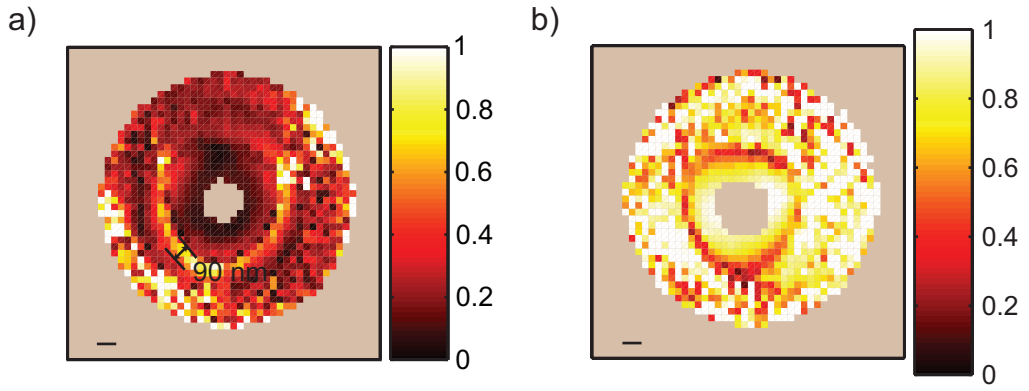

Figure 18: The measured degree of polarization P_2 of the light scattered by a single nanoparticle as a function of its position in the focal plane of the microscope objective. In a) the incident field is unpolarized and in b) fully polarized. The scale bar is 100 nm. At the center of the focus the detectors are saturated due to the high intensity and far away from the focus the intensity is too low to provide information about the polarization distribution. Hence, these areas are left out from the data.

dition number of the polarization analyzer, defined as $\|\mathbf{R}\|\|\mathbf{R}^{-1}\|$ where the matrix $\mathbf{R}$ has the elements R_{ij}, was 13.

Although the measurement method illustrated in Fig. 17 does not yield directly the 3D degree of polarization it gives indirect information about the polarization state in the focal region. Most importantly, because any two components of a field which is fully polarized in 3D are fully correlated, the electromagnetic field composed of such components is necessarily fully polarized as well. Likewise, an electromagnetic field composed of two components of a 3D unpolarized field is also unpolarized. The degree of polarization measured in the experiments is thus an indirect measure for how polarized the light in the focal region is. The full 3D coherence matrix of the light in the focal region can be obtained using the method illustrated in Fig. 17 if the photodiodes are replaced by position sensitive detectors.

The signals of the detectors of the polarization analyzer are proportional to the intensity of the polarization component corresponding to the specific detector integrated over the collection angle of the objective. The theoretically calculated distribution for the *measured* P_2 can thus be calculated by using the formalism of vector-wave focusing to obtain $\mathbf{\Phi}_3(\mathbf{r}, \omega)$. The coherence matrix measured with the polarization analyzer $\mathbf{\Phi}_2(\mathbf{r}', \mathbf{r}, \omega)$, and finally the measured P_2 then follows [Paper V].

Figure 18a) shows the measurement result for the case of unpolarized incident light. As expected from Sec. 4.2, we observe a ring around the focus

on which the degree of polarization of the scattered light is high. Outside the ring the degree of polarization has a low value consistent with the theoretical prediction.

For a fully polarized incident field the focal region field should also be fully polarized as there are, ideally, no elements that would introduce random fluctuations to the optical field. Indeed, the measured degree of polarization for fully polarized illumination shown in Fig. 18b) is high except along a ring around the focus with a radius of about 250 nm. On this ring the light seems to be almost unpolarized. This effect is an artifact of the measurement method. On these points the light in the focal region is polarized mainly along the optical axis so that the polarization distribution of the light scattered by the nanoparticle is cylindrically symmetric in the aperture of the objective. Such light is interpreted as unpolarized by the polarization analyzer of Fig. 17.

5 Summary and conclusions

The development of scanning near-field optical microscopy (SNOM) in the mid-1980s can be considered the birth of the field of nano optics although there exist earlier studies that would qualify in this category too. From this very focused beginning, the science of nano optics has grown explosively and can, to some extent, be said to have ceased to exist as a separate field of research. Instead, nano optics has made its way into many fields ranging from physics to life sciences. The properties of light on the nanoscale are studied in a wide variety of contexts, and, in structures ranging from individual molecules to nanopatterned surfaces which reveal fascinating optical properties. Optical means are used to manipulate and track nanoparticles and nanowires as well as isolated molecules, all much smaller than the wavelength of light. The diffraction limit which was seen to restrict optics to the microscale does not anymore seem like an unsurmountable obstacle.

This thesis concerns both the study of light on the nanoscale as well as the characterization of the optical properties of nanometer scale structures. These topics were explored experimentally and theoretically. A new method for studying metallic nanoparticles was developed and used to detect and spectrally characterize gold nanoparticles. It was shown that by combining supercontinuum confocal microscopy and interferometric detection, information about smaller than 10 nm diameter gold nanoparticles can be obtained. The developed method can also be extended to yield information about both the real and imaginary parts of the refractive index of the particle material.

Optical spectroscopy was also used to study the light transmission properties of subwavelength width slits fabricated in gold films. The experimental data was compared to numerical calculations and a good agreement was found. Based on the results from the experimental and theoretical research the mechanism of resonant light transmission was discussed. The transmission of light through the structure is mainly via the propagating TM-polarized mode. The influence of the structural parameters on the transmission spectrum could be explained by examining the properties of the mode. The sensitivity of the transmission spectrum to external disturbances was also investigated for sensing and switching applications.

The thesis also includes the first study of tight focusing of partially polarized electromagnetic beams. The polarization properties of the focal field were calculated for different polarization states of the incident field. It was found that even for an unpolarized incident field the focal region contains points where the field is fully polarized. This counterintuitive result was shown to be a geometric effect related to the focusing. The theoretical predictions were verified by experimentally measuring the distribution of the

degree of polarization in the focal plane of a high-NA microscope objective.

In this thesis only a limited number of aspects of the studied topics could be addressed. Each one of the investigations opens up many interesting questions. For example, supercontinuum confocal microscopy can be applied to study not only nanoparticles but also other structures. The combination of confocal microscopy and spectroscopy yields much more information than either method alone. The interferometric detection method has already been demonstrated to yield information about the material properties of nanoparticles. Developing further and applying this technique to study particles of different size and shape to determine the limit where bulk material parameters can not anymore be used to characterize matter would be a very interesting task. Using light scattering by a nanoparticle to probe the polarization properties of electromagnetic fields on the nanoscale opens up a multitude of research subjects. Questions of optical coherence in nanostructures have only recently been touched upon and mainly theoretically. The work performed in this thesis can be used to extend these studies to the experimental domain. This would undoubtedly lead to additional lines of research opening up.

References

[1] M. Ohtsu and H. Hori, *Near-Field Nano-Optics* (Kluwer Academic, New York, 1999).

[2] S. Kawata (Ed.), *Near-Field Optics and Surface Plasmon Polaritons* (Springer-Verlag, Berlin, 2001).

[3] F. de Fornel, *Evanescent Waves* (Springer, Berlin, 2001).

[4] D. Courjon, *Near-Field Microscopy and Near-Field Optics* (Imperial College Press, London, 2003).

[5] P. N. Prasad, *Nanophotonics* (John Wiley & Sons, New York, 2004).

[6] L. Novotny and B. Hecht, *Principles of Nano-Optics* (Cambridge University Press, Cambridge, UK, 2006).

[7] D. W. Pohl, W. Denk, and M. Lanz, "Optical stethoscopy: Image recording with resolution $\lambda/20$," Appl. Phys. Lett **44**, 651–653 (1984).

[8] A. Lewis, M. Isaacson, A. Harootunian, and A. Muray, "Development of a 500 Å spatial resolution light microscope I. light is efficiently transmitted through $\lambda/16$ diameter apertures," Ultramicroscopy **13**, 227–231 (1984).

[9] D. J. Barber and I. C. Freestone, "An investigation of the origin of the colour of the lycurgus cup by analytical transmission electron microscopy," Archaeometry **32**, 33–45 (1990).

[10] U. Kreibig and M. Vollmer, *Optical Properties of Metal Clusters* (Springer, Heidelberg, 1995).

[11] G. Mie, "Beitrage zur Optik trüber Medien speziell kolloidaler Metallösungen," Ann. Phys. **25**, 377–445 (1908).

[12] S. Nie and S. R. Emory, "Probing Single Molecules and Single Nanoparticles by Surface-Enhanced Raman Scattering," Science **274**, 1102-1106 (1997).

[13] J. J. Mock, D. R. Smith, and S. Schultz, "Local Refractive Index Dependence of Plasmon Resonance Spectra from Individual Nanoparticles," Nano Lett. **3**, 485–491 (2003).

[14] H. Raether, *Surface Plasmons on Smooth and Rough Surfaces and on Gratings* (Springer-Verlag, Berlin, 1988).

[15] W. L. Barnes, A. Dereux, and T. W. Ebbesen, "Surface plasmon subwavelength optics," Nature **424**, 824–830 (2003).

[16] A. V. Zayats and I. I. Smolyaninov, "Near-field photonics: surface plasmon polaritons and localized surface plasmons," J. Opt. A **5**, S16–S50 (2003).

[17] C. Genet and T. W. Ebbesen, "Light in tiny holes," Nature **445**, 39–46 (2007).

[18] S. W. Hell and J. Wichmann, "Breaking the diffraction resolution limit by stimulated emission," Opt. Lett. **19**, 780–782 (1994).

[19] E. Wolf, "Optics in terms of observable quantities," Nuovo Cimento **12**, 884–888 (1954).

[20] P. Roman and E. Wolf, "Correlation theory of stationary electromagnetic fields. Part I: the basic field equations," Nuovo Cimento **17**, 462–476 (1960).

[21] L. Mandel and E. Wolf, *Optical coherence and quantum optics* (Cambridge University Press, Cambridge, UK, 1995).

[22] C. Brosseau, *Fundamentals of Polarized Light: A Statistical Optics Approach* (John Wiley & Sons, New York, 1998).

[23] J. D Jackson, *Classical Electrodynamics* (John Wiley & Sons, New York, 1975).

[24] M. Born and E. Wolf, *Principles of Optics* (Pergamon Press, Oxford, 1980), sixth edition.

[25] M. Nieto-Vesperinas, *Scattering and diffraction in physical optics* (John Wiley & Sons, New York, 1991).

[26] J. Tervo, T. Setälä, and A. T. Friberg, "Theory of partially coherent electromagnetic fields in the space-frequency domain," J. Opt. Soc. Am. A **21**, 2205–2215 (2005).

[27] T. Setälä, A. Shevchenko, M. Kaivola, and A. T. Friberg, "Degree of polarization for optical near fields," Phys. Rev. E **66**, 016615 (2002).

[28] C. Brosseau and A. Dogariu, "Symmetry properties and polarization descriptors for an arbitrary electromagnetic wavefield" in *Progress in Optics* Vol. 49, E. Wolf ed. (Elsevier, 2006), pp. 315–380.

[29] N. W. Ashcroft and N. D. Mermin, *Solid State Physics* (Saunders College Publishing, Fort Worth, USA, 1976).

[30] M. A. Van Dijk, M. Lippitz, and M. Orrit. "Far-field optical microscopy of single metal nanoparticles." Acc. Chem. Research **38**, 594–601 (2005).

[31] L. A. Peyser, A. E. Vinson, A. P. Bartko, and R. M. Dickson, "Photoactivated Fluorescence from Individual Silver Nanoclusters," Science **291**, 103–106 (2001).

[32] D. Yelin, D. Oron, S. Thiberge, E. Moses, and Y. Silberberg, "Multiphoton plasmon-resonance microscopy," Opt. Express **11**, 1385–1391 (2003).

[33] R. A. Farrer, F. L. Butterfield, V. W. Chen, and J. T. Fourkas, "Highly Efficient Multiphoton-Absorption-Induced Luminescence from Gold Nanoparticles," Nano Lett. **5**, 1139–1142 (2005).

[34] K. Imura, T. Nagahara, and H. Okamoto, "Near-Field Two-Photon-Induced Photoluminescence from Single Gold Nanorods and Imaging of Plasmon Modes," J. Phys. Chem. B **109**, 13214–13220 (2005).

[35] S. Schultz, D. R. Smith, J. J. Mock, and D. A. Schultz, "Single-target molecule detection with nonbleaching multicolor optical immunolabels," Proc. Natl. Acad. U.S.A. **97**, 996–1001 (2000).

[36] C. Sönnichsen, S. Geier, N. E. Hecker, G. von Plessen, J. Feldmann, H. Ditlbacher, B. Lamprecht, J. R. Krenn, F. R. Aussenegg, V. Z-H. Chan, J. P. Spatz, and M. Möller, "Spectroscopy of single metallic nanoparticles using total internal reflection microscopy," Appl. Phys. Lett. **77**, 2949–2951 (2000).

[37] T. Itoh, T. Asahi, and H. Masuhara, "Femtosecond light scattering spectroscopy of single gold nanoparticles," Appl. Phys. Lett. **79**, 1667–1669 (2001).

[38] T. Klar, M. Perner, S. Grosse, G. von Plessen, W. Spirkl, and J. Feldmann, "Surface-Plasmon Resonances in Single Metallic Nanoparticles," Phys. Rev. Lett. **80**, 4249–4252 (1998).

[39] A. A. Mikhailovsky, M. A. Petruska, M. I. Stockman, and V. I. Klimov, "Broadband near-field interference spectroscopy of metal nanoparticles using a femtosecond white-light continuum," Opt. Lett. **28**, 1686–1688 (2003).

[40] J. S. Batchelder and M. A. Taubenblatt, "Interferometric detection of forward scattered light from small particles," Appl. Phys. Lett. **55**, 215–217 (1989).

[41] M. A. Taubenblatt and J. S. Batchelder, "Measurement of the size and refractive index of a small particle using the complex forward-scattered electromagnetic field," Appl. Opt. **30**, 4972–4979 (1991).

[42] Y. Matsuo and K. Sasaki, "Time-resolved Laser Scattering Spectroscopy of a Single Metallic Nanoparticle," Jpn. J. Appl. Phys. **40**, 6143–6147 (2001).

[43] P. Stoller, V. Jacobsen, and V. Sandoghdar, "Measurement of the complex dielectric constant of a single gold nanoparticle," Opt. Lett. **31**, 2474–2476 (2006).

[44] F. V. Ignatovich and L. Novotny, "Real-Time and Background-Free Detection of Nanoscale Particles," Phys. Rev. Lett. **96**, 013901 (2006).

[45] Y.-H. Liau, A. N. Unterreiner, Q. Chang, and N. F. Scherer, "Ultrafast Dephasing of Single Nanoparticles Studied by Two-Pulse Second-Order Interferometry," J. Phys. Chem. B **105**, 2135–2142 (2001).

[46] M. Lippitz, M. A. van Dijk, and M. Orrit, "Third-Harmonic Generation from Single Gold Nanoparticles," Nano Lett. **5**, 799–802 (2005).

[47] K. Mawatari, T. Kitamori, and T. Sawada, "Individual Detection of Single-Nanometer-Sized Particles in Liquid by Photothermal Microscope," Anal. Chem. **70**, 5037–5041 (1998).

[48] D. Boyer, P. Tamarat, A. Maali, B. Lounis, and M. Orrit, "Photothermal Imaging of Nanometer-Sized Metal Particles Among Scatterers," Science **297**, 1160–1163 (2002).

[49] S. Berciaud, L. Cognet, G. A. Blab, and B. Lounis, "Photothermal Heterodyne Imaging of Individual Nonfluorescent Nanoclusters and Nanocrystals," Phys. Rev. Lett. **93**, 257402 (2004).

[50] A. Arbouet, D. Christofilos, N. Del Fatti, F. Vallée, J. R. Huntzinger, L. Arnaud, P. Billaud, and M. Broyer, "Direct Measurement of the Single-Metal-Cluster Optical Absorption," Phys. Rev. Lett. **93**, 127401 (2004).

[51] T. W. Ebbesen, H. J. Lezec, H. F. Ghaemi, T. Thio, and P. A. Wolff, "Extraordinary optical transmission through sub-wavelength hole arrays," Nature **391**, 667–669 (1998).

[52] H. F. Ghaemi, T. Thio, D. E. Grupp, T. W. Ebbesen, and H. J. Lezec, "Surface plasmons enhance optical transmission through subwavelength holes," Phys. Rev. B **58**, 6779–6782 (1998).

[53] U. Shröter and D. Heitmann, "Surface-plasmon-enhanced transmission through metallic gratings," Phys. Rev. B **58**, 15419–15421 (1998).

[54] J. A. Porto, F. J. García-Vidal, and J. B. Pendry, "Transmission Resonances on Metallic Gratings with Very Narrow Slits," Phys. Rev. Lett. **83**, 2845–2848 (1999).

[55] D. E. Grupp, H. J. Lezec, T. W. Ebbesen, K. M. Pellerin, and T. Thio, "Crucial role of metal surface in enhanced transmission through subwavelength apertures," Appl. Phys. Lett. **77**, 1569–1571 (2000).

[56] E. Popov, M. Nevière, S. Enoch, and R. Reinisch, "Theory of light transmission through subwavelength periodic hole arrays," Phys. Rev. B **62**, 16100–16108 (2000).

[57] Ph. Lalanne, J. P. Hugonin, S. Astilean, M. Palamaru, and K. D. Möller, "One-mode model and Airy-like formulae for one-dimensional metallic gratings," J. Opt. A **2**, 48–51 (2000).

[58] S. Astilean, Ph. Lalanne, and M. Palamaru, "Light transmission through metallic channels much smaller than the wavelength," Opt. Commun. **175**, 265–273 (2000).

[59] H. E. Went, A. P. Hibbins, J. R. Sambles, C. R. Lawrence, and A. P. Crick, "Selective transmission through very deep zero-order metallic gratings at microwave frequencies," Appl. Phys. Lett. **77**, 2789–2791 (2000).

[60] S. Collin, F. Pardo, R. Teissier, and J.-L. Pelouard, "Strong discontinuities in the complex photonic band structure of transmission metallic gratings," Phys. Rev. B **63**, 033107 (2001).

[61] L. Salomon, F. Grillot, A. Zayats, and F. de Fornel, "Near-Field Distribution of Optical Transmission of Periodic Subwavelength Holes in a Metal Film," Phys. Rev. Lett. **86**, 1110–1113 (2001).

[62] L. Martín-Moreno, F. J. García-Vidal, H. J. Lezec, K. M. Pellerin, T. Thio, J. B. Pendry, and T. W. Ebbesen, "Theory of Extraordinary Optical Transmission through Subwavelength Hole Arrays," Phys. Rev. Lett. **86**, 1114–1117 (2001).

[63] T. Thio, K. M. Pellerin, R. A. Linke, H. J. Lezec, and T. W. Ebbesen, "Enhanced light transmission through a single subwavelength aperture," Opt. Lett. **26**, 1972–1974 (2001).

[64] Y. Takakura, "Optical Resonance in a Narrow Slit in a Thick Metallic Screen," Phys. Rev. Lett. **86**, 5601–5603 (2001).

[65] Q. Cao and Ph. Lalanne, "Negative Role of Surface Plasmons in the Transmission of Metallic Gratings with Very Narrow Slits," Phys. Rev. Lett. **88**, 057403 (2002).

[66] F. I. Baida and D. Van Labeke, "Light transmission by subwavelength annular aperture arrays in metallic films," Opt. Commun. **209**, 17–22 (2002).

[67] P.-K. Wei, H.-L. Chou, and W.-S. Fann, "Optical near field in nanometallic slits," Opt. Express **10**, 1418–1424 (2002).

[68] A. P. Hibbins, J. R. Sambles, and C. R. Lawrence, "Gratingless enhanced microwave transmission through a subwavelength aperture in a thick metal plate," Appl. Phys. Lett. **81**, 4661–4663 (2002).

[69] J. Gómez Rivas, C. Schotsch, P. Haring Bolivar, and H. Kurz, "Enhanced transmission of THz radiation through subwavelength holes," Phys. Rev. B **68**, 201306(R) (2003).

[70] F. J. García-Vidal, H. J. Lezec, T. W. Ebbesen, and L. Martín-Moreno, "Multiple Paths to Enhance Optical Transmission through a Single Subwavelength Slit," Phys. Rev. Lett. **90**, 213901 (2003).

[71] B. Dragnea, J. M. Szarko, S. Kowarik, T. Weimann, J. Feldmann, and S. R. Leone, "Near-Field Surface Plasmon Excitation on Structured Gold Films," Nano Lett. **3**, 3–7 (2003).

[72] A. Degiron, H. J. Lezec, N. Yamamoto, and T. W. Ebbesen, "Optical transmission properties of a single subwavelength aperture in a real metal," Opt. Commun. **239**, 61–66 (2004).

[73] J. Prikulis, P. Hanarp, L. Olofsson, D. Sutherland, and M. Käll, "Optical Spectroscopy of Nanometric Holes in Thin Gold Films," Nano Lett. **4**, 1003–1007 (2004).

[74] S. H. Garrett, L. H. Smith, and W. L. Barnes, "Fluorescence in the presence of metallic hole arrays," J. Mod. Opt. **52**, 1105–1122 (2005).

[75] J. Wenger, P.-F. Lenne, E. Popov, and H. Rigneault, "Single molecule fluorescence in rectangular nano-apertures," Opt. Express **13**, 7035–7044 (2005).

[76] H. Rigneault, J. Capoulade, J. Dintinger, J. Wenger, N. Bonod, E. Popov, T. W. Ebbesen, and P.-F. Lenne, "Enhancement of Single-Molecule Fluorescence Detection in Subwavelength Apertures," Phys. Rev. Lett. **95**, 117401 (2005).

[77] M. Leutenegger, M. Gösch, A. Perentes, P. Hoffmann, O. J. F. Martin, and T. Lasser, "Confining the sampling volume for Fluorescence Correlation Spectroscopy using a sub-wavelength sized aperture," Opt. Express **14**, 956–969 (2006).

[78] H. J. Lezec, A. Degiron, E. Devaux, R. A. Linke, L. Martin-Moreno, F. J. Garcia-Vidal, and T. W. Ebbesen, "Beaming Light from a Subwavelength Aperture," Science **297**, 820–822 (2002).

[79] H. Cao, A. Agrawal, and A. Nahata, "Controlling the transmission resonance lineshape of a single subwavelength aperture," Opt. Express **13**, 763–769 (2005).

[80] C.-L. Pan, C.-F. Hsieh, R.-P. Pan, M. Tanaka, F. Miyamaru, M. Tani, and M. Hangyo, "Control of enhanced THz transmission through metallic hole arrays using nematic liquid crystal," Opt. Express **13**, 3921–3930 (2005).

[81] J. Dintinger, I. Robel, P. V. Kamat, C. Genet, and T. W. Ebbesen, "Terahertz All-Optical Molecule-Plasmon Modulation," Adv. Mater. **18**, 1645–1648 (2006).

[82] J. Dintinger, S. Klein, and T. W. Ebbesen, "Molecule-Surface Plasmon Interactions in Hole Arrays: Enhanced Absorption, Refractive Index Changes, and All-Optical Switching," Adv. Mater. **18**, 1267–1270 (2006).

[83] S. Collin, F. Pardo, R. Teissier, and J.-L. Pelouard, "Efficient light absorption in metal-semiconductor-metal nanostructures," Appl. Phys. Lett. **85**, 194–196 (2004).

[84] T. Ishi, J. Fujikata, K. Makita, T. Baba, and K. Ohashi, "Si Nano-Photodiode with a Surface Plasmon Antenna," Jpn. J. Appl. Phys **44**, L364–L366 (2005).

[85] S. Shinada, J. Hashizume, and F. Koyama, "Surface plasmon resonance on microaperture vertical-cavity surface-emitting laser with metal grating," Appl. Phys. Lett. **83**, 836–838 (2003).

[86] J. Bravo-Abad, F. J. García-Vidal, and L. Martín-Moreno, "Wavelength de-multiplexing properties of a single aperture flanked by periodic arrays of indentations," Photonics and Nanostructures **1**, 55–62 (2003).

[87] C. Liu, V. Kamaev, and Z. V. Vardeny, "Efficiency enhancement of an organic light-emitting diode with a cathode forming two-dimensional periodic hole array," Appl. Phys. Lett. **86**, 143501 (2005).

[88] K. A. Tetz, L. Pang, and Y. Fainman, "High-resolution surface plasmon resonance sensor based on linewidth-optimized nanohole array transmittance," Opt. Lett. **31**, 1528–1530 (2006).

[89] K.-L. Lee, C.-W. Lee, W.-S. Wang, and P.-K. Wei, "Sensitive biosensor array using surface plasmon resonance on metallic nanoslits," J. Biomedical Optics **12**, 044023 (2007).

[90] W. Srituravanich, N. Fang, C. Sun, Q. Luo, and X. Zhang, "Plasmonic Nanolithography," Nano Lett. **4**, 1085–1088 (2004).

[91] T. Xu, C. Du, C. Wang, and X. Luo, "Subwavelength imaging by metallic slab lens with nanoslits," Appl. Phys. Lett. **91**, 201501 (2007).

[92] M. Airola, Y. Liu, and S. Blair, "Second-harmonic generation from an array of sub-wavelength metal apertures," J. Opt. A **7**, S118–S123 (2005).

[93] A. G. Brolo, E. Arctander, R. Gordon, B. Leathem, and K. L. Kavanagh, "Nanohole-Enhanced Raman Scattering," Nano Lett. **4**, 2015–2018 (2004).

[94] J. Wenger, J. Dintinger, N. Bonod, E. Popov, P.-F. Lenne, T. W. Ebbesen, and H. Rigneault, "Raman scattering and fluorescence emission in a single nanoaperture: Optimizing the local intensity enhancement," Opt. Commun. **267**, 224–228 (2006).

[95] C. F. Bohren and D. R. Huffman, *Absorption and Scattering of Light by Small Particles* (John Wiley & Sons, New York, 1983).

[96] P. B. Johnson and R. W. Christy, "Optical Constants of the Noble Metals," Phys. Rev. B **6**, 4370–4379 (1972).

[97] J. Lindberg (private communication).

[98] G. Raschke, S. Kowarik, T. Franzl, C. Sönnichsen, T. A. Klar, J. Feldmann, A. Nichtl, and K. Kürzinger, "Biomolecular Recognition Based on Single Gold Nanoparticle Light Scattering," Nano Lett. **3**, 935–938 (2003).

[99] A. D. McFarland and R. P. Van Duyne, "Single Silver Nanoparticles as Real-Time Optical Sensors with Zeptomole Sensitivity," Nano Lett. **3**, 1057–1062 (2003).

[100] T. Kalkbrenner, U. Håkanson, and V. Sandoghdar, "Tomographic Plasmon Spectroscopy of a Single Gold Nanoparticle," Nano Lett. **4**, 2309–2314 (2004).

[101] N. Morita, T. Tanaka, T. Yamasaki, and Y. Nakanishi, "Scattering of a Beam Wave by a Spherial Object," IEEE. Trans. Ant. Prop. **16**, 724–727 (1968).

[102] J. K. Ranka, R. S. Windeler, and A. J. Stentz, "Visible continuum generation in air-silica microstructure optical fibers with anomalous dispersion at 800 nm," Opt. Lett. **25**, 25–27 (2000).

[103] T. Wilson, R. Juškaitis, and P. Higdon, "The imaging of dielectric point scatterers in conventional and confocal polarisation microscopes," Opt. Comm. **141**, 298–313 (1997).

[104] H. A. Bethe, "Theory of Diffraction by Small Holes," Phys. Rev. **66**, 163–182 (1944).

[105] J. Salvi, M. Roussey, F. I. Baida, M.-P. Bernal, A. Mussot, T. Sylvestre, H. Maillotte, D. Van Labeke, A. Perentes, I. Utke, C. Sandu, P. Hoffmann, and B. Dwir, "Annular aperture arrays: study in the visible

region of the electromagnetic spectrum," Opt. Lett. **30**, 1611–1613 (2005).

[106] S.-H. Chang, S. K. Gray, and G. C. Schatz, "Surface plasmon generation and light transmission by isolated nanoholes and arrays of nanoholes in thin metal films," Opt. Express **13**, 3150–3165 (2005).

[107] E. Popov, N. Bonod, M. Nevière, H. Rigneault, P. F. Lenne, and P. Chaumet, "Surface plasmon excitation on a single subwavelength hole in a metallic sheet," Appl. Opt. **44**, 2332–2337 (2005).

[108] E. Popov, M. Nevière, P. Boyer, and N. Bonod, "Light transmission through a subwavelength hole," Opt. Commun. **255**, 338–348 (2005).

[109] P. K. Banerjee and R. Butterfield, *Boundary element methods in engineering science* (McGraw-Hill, London, 1981).

[110] C. A. Brebbia, J. F. C. Telles, and L. C. Wrobel, *Boundary element techniques: theory and applications in engineering* (Springer, Berlin, 1984).

[111] L. Ram-Mohan and L. Ramdas, *Finite Element and Boundary Element Applications in Quantum Mechanics* (Oxford University Press, Oxford, 2002).

[112] I. P. Kaminow, W. L. Mammel, and H. P. Weber, "Metal-Clad Optical Waveguides: Analytical and Experimental Study," Appl. Opt. **13**, 396–405 (1974).

[113] R. Gordon, "Light in a subwavelength slit in a metal: Propagation and reflection," Phys. Rev. B **73**, 153405 (2006).

[114] "Microscope" In Encyclopœdia Britannica. Retrieved July 18, 2008, from Encyclopœdia Britannica Online: http://www.britannica.com/EBchecked/topic/380582/microscope (2008).

[115] "G. B. Amici" In Encyclopœdia Britannica. Retrieved July 18, 2008, from Encyclopœdia Britannica Online: http://www.britannica.com/EBchecked/topic/20544/Giovanni-Battista-Amici (2008).

[116] E. Abbe, "Beiträge zur Theorie des Mikroskops und der mikroskopischen Wahrnehmung," Arch. Mikroskop. Anat. **9**, 413–468 (1873).

[117] H. Volkmann, "Ernst Abbe and His Work," Appl. Opt. **5**, 1720–1731 (1966).

[118] Lord Rayleigh, "On the Theory of Optical images, with Special Reference to the Microscope," Phil. Mag. **42**, 167–195 (1896).

[119] F. Zernike, "Das Phasenkontrastverfahren bei der mikroskopischen Beobachtung," Phys. Z. **36**, 848–851 (1935).

[120] R. Zsigmondy, *Zur Erkenntnis der Kolloide* (G. Fischer, Jena, 1905).

[121] G. Nomarski, "Microintereféromètre différentiel à ondes polarisées," J. Phys. Rad. **16**, S9–S13 (1955).

[122] A. H. Coons, H. J. Creech, and R. Jones, "Immunological properties of an antibody containing a fluorescent group," Proc. Soc. Exp. Biol. Med. **47**, 200–202 (1941).

[123] A. H. Coons, H. J. Creech, R. Jones, and E. Berliner, "The demonstration of pneumococcal antigen in tissues by the use of fluorescent antibody," J. Immunol. **45**, 159–170 (1942).

[124] E. Betzig, G. H. Patterson, R. Sougrat, O. W. Lindwasser, S. Olenych, J. S. Bonifacino, M. W. Davidson, J. Lippincott-Schwartz, and H. F. Hess, "Imaging Intracellular Fluorescent Proteins at Nanometer Resolution," Science **313**, 1642–1645 (2006).

[125] M. J. Rust, M. Bates, and X. Zhuang, "Sub-diffraction-limit imaging by stochastic optical reconstruction microscopy (STORM)," Nature Methods **3**, 793–796 (2006).

[126] M. G. L. Gustafsson, "Surpassing the lateral resolution limit by a factor of two using structured illumination microscopy," J. Microscopy **198**, 82–87 (2000).

[127] E. H. Synge, "Suggested method for extending microscopic resolution into the ultramicroscopic region," Phil. Mag. **6**, 356–362 (1928).

[128] E. A. Ash and G. Nicholls, "Super-resolution aperture scanning microscope," Nature **237**, 510–512 (1972).

[129] G. Binnig and H. Rohrer, "Scanning Tunneling Microscopy," Helvetica Physica Acta **55**, 726–735 (1982).

[130] G. Binnig, C. F. Quate, and Ch. Gerber, "Atomic Force Microscope," Phys. Rev. Lett. **56**, 930–933 (1986).

[131] C. C. Williams and H. K. Wickramasinghe, "Scanning thermal profiler," Appl. Phys. Lett. **49**, 1587–1589 (1986).

[132] C. M. Mate, G. M. McClelland, R. Erlandsson, and S. Chiang, "Atomic-Scale Friction of a Tungsten Tip on a Graphite Surface," Phys. Rev. Lett. **59**, 1942–1945 (1987).

[133] Y. Martin and H. K. Wickramasinghe, "Magnetic imaging by 'force microscopy' with 1000 Å resolution," Appl. Phys. Lett. **50**, 1455–1457 (1987).

[134] Y. Martin, D. W. Abraham, and H. K. Wickramasinghe, "High-resolution capacitance measurement and potentiometry by force microscopy," Appl. Phys. Lett. **52**, 1103–1105 (1988).

[135] M. Nonnenmacher, M. P. O'Boyle, and H. K. Wickramasinghe, "Kelvin probe force microscopy," Appl. Phys. Lett. **58**, 2921–2923 (1991).

[136] D. Courjon, K. Sarayeddine, and M. Spajer, "Scanning tunneling optical microscopy," Opt. Commun. **71**, 23–28 (1989).

[137] R. C. Reddick, R. J. Warmack, and T. L. Ferrell, "New form of scanning optical microscopy," Phys. Rev. B **39**, 767–770 (1989).

[138] M. Minsky, "Microscopy Apparatus," United States Patent 3,013,467, December 19, 1961.

[139] W. Denk, J. H. Strickler, and W. W. Webb, "Two-photon laser scanning fluorescence microscopy," Science **248**, 73–76 (1990).

[140] M. Petráň, M. Hadravský, M. D. Egger, and R. Galambos, "Tandem-Scanning Reflected-Light Microscope," J. Opt. Soc. Am. **58**, 661–664 (1968).

[141] V. S. Ignatowsky, "Diffraction by an objective lens of arbitrary aperture," Trans. Opt. Inst. **1**, 1–30 (1919).

[142] H. H. Hopkins, "The Airy Disc Formula For Systems of High Relative Aperture," Proc. Phys. Soc. **55**, 116–129 (1943).

[143] B. Richards, "Diffraction in systems of high relative aperture" in *Proceedings of a symposium on Astronomical optics and related subjects : held in the University of Manchester, April 19th-22nd, 1955*, Zdeněk Kopal ed. (North-Holland, 1956), pp. 352–359.

[144] B. Richards and E. Wolf, "Electromagnetic diffraction in optical systems II. Structure of the image field in an aplanatic system," Proc. Roy. Soc. A **253**, 358–379 (1959).

[145] R. Dorn, S. Quabis, and G. Leuchs, "The focus of light–linear polarization breaks the rotational symmetry of the focal spot," J. Mod. Opt. **50**, 1917–1926 (2003).

[146] H. H. Hopkins, "Resolving Power of the Microscope using Polarized Light," Nature **155**, 275–275 (1945).

[147] C. J. R. Sheppard, "Focal distributions and Hertz potentials," Opt. Commun. **160**, 191–194 (1999).

[148] K. S. Youngworth and T. G. Brown, "Focusing of high numerical aperture cylindrical-vector beams," Opt. Express **7**, 77–87 (2000).

[149] S. Quabis, R. Dorn, M. Eberler, O. Glöckl, and G. Leuchs, "Focusing light to a tighter spot," Opt. Comm. **179**, 1–7 (2000).

[150] Q. Zhan and J. R. Leger, "Focus shaping using cylindrical vector beams," Opt. Express **10**, 324–331 (2001).

[151] D. Ganic, X. Gan, and M. Gu, "Focusing of doughnut laser beams by a high numerical-aperture objective in free space," Opt. Express **11**, 2747–2752 (2003).

[152] R. Dorn, S. Quabis, and G. Leuchs, "Sharper Focus for a Radially Polarized Light Beam," Phys. Rev. Lett. **91**, 233901 (2003).

[153] J. Lekner, "Polarization of tightly focused laser beams," J. Opt. A **5**, 6–14 (2003).

[154] R. Borghi, M. Santarsiero, and M. A. Alonso, "Highly focused spirally polarized beams," J. Opt. Soc. Am. A **22**, 1420–1431 (2005).

[155] I. J. Cooper, M. Roy, and C. J. R. Sheppard, "Focusing of pseudoradial polarized beams," Opt. Express **13**, 1066–1071 (2005).

[156] D. W. Diehl, R. W. Schoonover, and T. D. Visser, "The structure of focused, radially polarized fields," Opt. Express **14**, 3030–3038 (2006).

[157] W. Chen and Q. Zhan, "Three-dimensional focus shaping with cylindrical vector beams," Opt. Commun. **265**, 411–417 (2006).

[158] B. Sick, B. Hecht, and L. Novotny, "Orientational imaging of single molecules by annular illumination," Phys. Rev. Lett. **85**, 4482–4485 (2000).

[159] L. Novotny, M. R. Beversluis, K. S. Youngworth, and T. G. Brown, "Longitudinal field modes probed by single molecules," Phys. Rev. Lett. **86**, 5251–5254 (2001).

[160] S. K. Rhodes, K. A. Nugent, and A. Roberts, "Precision measurement of the electromagnetic fields in the focal region of a high-numerical-aperture lens using a tapered fiber probe," J. Opt. Soc. Am. A **19**, 1689–1693 (2002).

[161] B. H. Jia, X. S. Gan, and M. Gu, "Direct observation of a pure focused evanescent field of a high numerical aperture objective lens by scanning near-field optical microscopy," Appl. Phys. Lett. **86**, 131110 (2005).

[162] H. Ling and S.-W. Lee, "Focusing of electromagnetic waves through a dielectric interface," J. Opt. Soc. Am. A **1**, 965–973 (1984).

[163] S. W. Hell and E. H. K. Stelzer, "Lens Aberrations in Confocal Fluorescence Microscopy" in *Handbook of Biological Confocal Microscopy*, J. B. Pawley ed. (Plenum Press, 1995), pp. 347–354.

[164] J. J. Stamnes and D. Jiang, "Focusing of electromagnetic waves into a uniaxial crystal," Opt. Commun. **150**, 251–262 (1998).

[165] D. P. Biss and T. G. Brown, "Cylindrical vector beam focusing through a dielectric interface," Opt. Express **9**, 490–497 (2001).

[166] L. E. Helseth, "Roles of polarization, phase and amplitude in solid immersion lens systems," Opt. Commun. **191**, 161–172 (2001).

[167] J. J. Stamnes, G. S. Sithambaranathan, M. Jain, J. K. Lotsberg, and V. Dhaylan, "Focusing of electromagnetic waves into a biaxial crystal," Opt. Commun. **226**, 107–123 (2003).

[168] L. A. Chernov, *Wave Propagation in Random Medium, Part III* (McGraw-Hill, New York, 1960).

[169] A. T. Friberg and J. Turunen, "Imaging of Gaussian Schell-model sources," J. Opt. Soc. Am. A **5**, 713–720 (1988).

[170] W. Wang, A. T. Friberg, and E. Wolf, "Focusing of partially coherent light in systems of large Fresnel numbers," J. Opt. Soc. Am. A **14**, 491–496 (1997).

[171] J. J. Stamnes, *Waves in Focal Regions* (Adam Hilger, Bristol and Boston, 1986).

[172] M. E. J. Friese, T. A. Nieminen, N. R. Heckenberg, and H. Rubinsztein-Dunlop, "Optical alignment and spinning of laser-trapped microscopic particles," Nature **394**, 348–350 (1998).

[173] S. A. Empedocles, R. Neuhauser, and M. G. Bawendi, "Three-dimensional orientation measurements of symmetric single chromophores using polarization microscopy," Nature **399**, 126–130 (1999).

[174] T. Kalkbrenner, M. Ramstein, J. Mlynek, and V. Sandoghdar, "A single gold particle as a probe for apertureless scanning near-field optical microscopy," J. Microsc. **202**, 72–76 (2001).

Abstracts of publications I–V

I. We combine confocal microscopy using supercontinuum laser illumination and an interferometric detection technique to identify single nanoparticles of diameter below 10 nm. Spectral analysis of the signal allows us to record the plasmon resonance of a single nanoparticle. Our results hold great promise for fundamental studies of the optical properties of single metal clusters and for their use in biophysical applications.

II. We analyze the spectral properties of resonant transmission of light through a sub-wavelength slit in a metal film. We show that the enhanced transmission can be understood in terms of interfering surface-wave-like modes propagating in the slit. We characterize the effect of geometrical and material properties of the slit on the transmission spectrum. Furthermore, we show that the wavelength of the transmission resonance strongly depends on the surrounding medium. This effect may be utilized in sensors, imaging, and the detection of, e.g. biomolecules.

III. We perform a systematic study of the resonant transmission of visible and near-infrared (NIR) light through a single subwavelength slit in a gold film when the parameters defining the structure are varied. We further examine the optical properties of a related nanostructure, a cross with subwavelength sized features. Focused ion beam (FIB) milling was used to fabricate nanoslits and crosses with linewidths ranging from 26 nm to 85 nm. The dimensions of the structure are found to affect strongly the transmittance spectrum. For example, as the slit becomes narrower the resonance is observed to both sharpen and shift significantly. Our observations are in good agreement with our earlier numerical calculations on the optical properties of nanoslits.

IV. We analyze the degree of polarization of random, statistically stationary electromagnetic fields in the focal region of a high-numerical-aperture imaging system. The Richards-Wolf theory for focusing is employed to compute the full 3×3 electric coherence matrix, from which the degree of polarization is obtained by using a recent definition for general three-dimensional electromagnetic waves. Significant changes in the state of partial polarization, compared with that of the incident illumination, are observed. For example, a wave consisting of two orthogonal and uncorrelated incident-electric-field components produces rings of full polarization in the focal plane. These effects are

explained by considering the distribution of the spectral densities of the three electric field components as well as the correlations between them.

V. The polarization of light is important in a great variety of optical phenomena, ranging from transmission, reflection and scattering to polarimetric imaging of scenes and quantum-mechanical selection rules of atomic and molecular transitions. Among some less-well-known phenomena that illustrate the vectorial nature of light are the Pancharatnam[1] (or geometric[2]) phase, singularities in the polarization pattern of clear sky[3] and polarization of microwave background radiation[4]. Here, we examine the partial polarization of focused light. We experimentally demonstrate a rather surprising phenomenon, where the focusing of unpolarized light results in rings of full polarization in the focal plane of the focusing optics. The polarization rings are imaged with a resolution of < 100 nm by probing the focal region using a gold nanoparticle.